BeamSync: Over-The-Air Synchronization for Distributed Massive MIMO Systems

Unnikrishnan Kunnath Ganesan, *Graduate Student Member, IEEE,*
Rimalapudi Sarvendranath, *Member, IEEE,*
Erik G. Larsson, *Fellow, IEEE*

***Abstract*—In distributed massive multiple-input multiple-output (MIMO) systems, multiple geographically separated access points (APs) communicate simultaneously with a user, leveraging the benefits of multi-antenna coherent MIMO processing and macro-diversity gains from the distributed setups. However, time and frequency synchronization of the multiple APs is crucial to achieve good performance and enable joint precoding. In this paper, we analyze the synchronization requirement among multiple APs from a reciprocity perspective, taking into account the multiplicative impairments caused by mismatches in radio frequency (RF) hardware. We demonstrate that a phase calibration of reciprocity-calibrated APs is sufficient for the joint coherent transmission of data to the user. To achieve synchronization, we propose a novel over-the-air synchronization protocol, named BeamSync, to calibrate the geographically separated APs without sending any measurements to the central processing unit (CPU) through fronthaul. We show that sending the synchronization signal in the dominant direction of the channel between APs is optimal. Additionally, we derive the optimal phase and frequency offset estimators. Simulation results indicate that the proposed BeamSync method enhances performance by 3 dB when the number of antennas at the APs is doubled. Moreover, the method performs well compared to traditional beamforming techniques.**

***Index Terms*—Massive MIMO, distributed MIMO, beamforming, synchronization, reciprocity.**

I. Introduction

MASSIVE multiple-input multiple-output (MIMO) introduced in [2], has grown into the leading physical layer technology for fifth generation (5G) and beyond 5G wireless systems. Massive MIMO uses many antennas at the access point (AP) and leverages time division duplexing (TDD) to obtain channel state information (CSI) by exploiting the channel reciprocity. It serves multiple users on the same-time frequency resources and controls the multi-user interference through spatial precoding [3]. To meet the increasing demand of wireless traffic, dense deployment of APs in the same coverage area is considered, creating small cells [4], [5]. However, extreme densification causes intercell interference and to mitigate it, distributed networks are used [6]–[9]. Large numbers of coordinated APs are distributed over a large coverage area and connected to a central processing unit (CPU) through a fronthaul to form a distributed network. Distributed massive MIMO or cell-free massive MIMO [5], [10] is a distributed network topology that blends in the advantages of massive MIMO and ultra-densification.

Distributed massive MIMO relies on two important assumptions: channel reciprocity and synchronization of distributed transmitters. The TDD architecture allows the CSI requirement only at the AP to provide data transmission to users without the requirement of CSI at the receiver. The propagation channel from the antenna to the antenna is reciprocal; however, transmitter and receiver hardware are not and thus introducing a multiplicative gain with an unknown amplitude scaling and phase shift between the uplink and downlink channels. This makes the channel non-reciprocal in practice. For distributed massive MIMO, it suffices to calibrate the phases of reciprocity-calibrated APs to achieve coherent downlink transmission. A TDD reciprocity calibration method was proposed in [11] for collocated massive MIMO. A channel reciprocity calibration method for industrial massive MIMO was proposed in [12], which involves incorporating the radio frequency (RF) impairment report into the power headroom report. In [13], a novel inter-cluster combining method was proposed for reciprocity calibration in distributed massive MIMO, which enhances the signal-to-noise ratio (SNR) of the sounding reference signals. In [14], a gradual method for channel non-reciprocity calibration is proposed, which involves the estimation of uplink channels, after which APs are sequentially calibrated in a particular order. The ordering is computed based on AP-user channel strengths.

Synchronizing a receiver and transmitter for coherent data transmission is a well-known problem and efficient solutions exist in the literature [15]–[18]. However, the synchronization techniques developed for a point-to-point communication system do not extend directly to a distributed communication system. Each distributed AP is equipped with a reference crystal oscillator to generate its clocks. Due to mismatches in the reference oscillator circuits, different transceivers generate different clocks. The drift and the jitter in the clock in different transmitters affect the coherent combining of signals at the

Manuscript received January 25, 2023; revised May 22, 2023 and August 22, 2023; accepted November 18, 2023. This work was supported in part by ELLIIT and in part by the REINDEER project of the European Union's Horizon 2020 research and innovation programme under grant agreement No. 101013425. A part of this article was presented at 25th International ITG Workshop on Smart Antennas (WSA 2021) [1]. The editor coordinating the review of this article and approving it for publication was Dr. Chao-Kai Wen. (*Corresponding author: Unnikrishnan Kunnath Ganesan.*)

Unnikrishnan Kunnath Ganesan and Erik G. Larsson are with the Department of Electrical Engineering (ISY), Linköping University, 581 83 Linköping, Sweden (e-mail: unnikrishnan.kunnath.ganesan@liu.se; erik.g.larsson@liu.se).

Rimalapudi Sarvendranath is with Department of Electrical Engineering at the Indian Institute of Technology, Tirupati, India (email: sarvendranath@iitp.ac.in).

Digital Object Identifier XX

users. To fully realize the benefits of distributed MIMO, and especially perform joint coherent beamforming from multiple APs to users, it is essential that the participating APs are frequency and phase aligned. While GPS could be used for frequency alignment in some deployments, for indoor environments synchronization with GPS may not be practical. Most theoretical works on distributed massive MIMO assumes perfect synchronization [5], [10], [19]–[22]. However, the assumption of perfect reciprocity calibration, and perfect phase and frequency synchronization of carrier is not very practical. The problems of achieving channel reciprocity calibration and synchronization in a distributed massive MIMO are entangled with each other. In this paper, we consider reciprocity calibration and propose methods to synchronize distributed APs to enable coherent transmission to user equipment (UE).

The CPU fronthaul network is unable to provide the timing and phase information to the APs and with unknown multiplicative gains from hardware, it becomes harder to synchronize the distributed APs through a fronthaul network. To address this issue, over-the-air synchronization methods were studied in [23]–[31]. Distributed coherent beamforming from multiple transmitters to a single user is studied in [23], [24] and the implementation of these ideas is studied in [25]–[27]. These works are based on a master-slave protocol, where a master AP transmits a tone to slave APs for frequency synchronization and the UE performs feedback signaling for phase synchronization. In practice, it is desirable to design a synchronization method without involving UEs to enable legacy devices without implementing any new protocols in the new network and to save power. In the AirSync technique studied in [28], a master AP transmits out-of-band pilots continuously to all the slave APs, which receive them through a dedicated receive antenna. The slave APs keep track of the incoming phase offset from the master AP and compensates it during the data transmission. During this phase compensation, a constant phase offset coming from the channel between master and slave APs, which is not compensated, becomes part of channel estimates. This assumes that the transmit and receive RF chains of each transceiver are perfectly calibrated both in amplitude and phase, which need not necessarily be practical. The AirShare technique proposed in [30] uses a dedicated emitter to transmit two low-frequency tones over the air and the distributed APs use a dedicated circuit to receive these tones and generate their reference signal with the frequency equal to the difference of the two tones. This technique is robust to variations in temperature and supply voltage at the emitter. However, it does not compensate for phase impairments from the hardware. To provide synchronization in large distributed networks, [31] considers a few APs as anchor APs that exchange pilot signals with each other, and the frequency and timing estimates are sent to the CPU through the fronthaul to estimate the correcting factors. The other APs need to synchronize with the nearest anchor AP using the master-slave approach. In [32], the calibration data are collected through a beam-sweep approach between all pairs of the participating APs and are sent to the CPU. An alternating optimization procedure is proposed to estimate the calibration coefficients and the complexity increases with the number of participating APs.

In this paper, we consider a generic scenario where transmit and receive gains in the same RF chain are different due to internal clocking structures and manufacturing differences. A relative phase calibration of reciprocity-calibrated APs with one of the APs suffices for the coherent combining of signals at the user, thereby achieving the benefits of distributed systems. The specific contributions of this paper can be summarized as follows:

- We propose a novel over-the-air synchronization technique, which we call *BeamSync*, to synchronize the phase and carrier frequency between distributed APs without the involvement of a UE. Each AP is equipped with a single local oscillator (LO). The main practical use case for BeamSync is to calibrate the phases of two different APs relative to one another such that these APs can perform joint coherent beamforming on downlink. BeamSync can synchronize the phase and frequency of distributed APs without any estimation of the channel between APs and does not require the transmission of any measurements to the CPU through fronthaul.
- We analytically derive the non-linear least squares (NLS) estimator for the phase offset between distributed APs and propose a simple phase offset estimator which performs close to the NLS estimator at a high SNR.
- We analytically derive the estimator for the frequency offset between distributed APs based on BeamSync. (A preliminary version of the same was published in the conference paper [1] considering perfect channel reciprocity.)
- We analytically show that the synchronization signals should be beamformed in the dominant direction of the effective channel in which the signal is received.
- Through simulations, we show that BeamSync can achieve good phase calibration even in the presence of phase noise. Also, BeamSync performs well compared to the traditional fixed grid of beams beamforming techniques. Moreover, we show that the performance of BeamSync improves by 3 dB when doubling the number of antennas at the AP for a fixed root mean square error (RMSE) requirement.

The rest of the paper is organized as follows. Section II discusses the system model considered in this paper. BeamSync for phase synchronization of distributed multi-antenna systems is presented in Section III and the frequency synchronization in Section IV. Numerical results and the performance of the BeamSync protocol are discussed in Section V. Finally, concluding remarks are given in Section VI.

Notations: Bold lowercase letters are used to denote vectors and bold uppercase letters are used to denote matrices. $\mathbb{R}$ and $\mathbb{C}$ denote the set of real and complex numbers, respectively. For a matrix $\mathbf{A}$, $\mathbf{A}^*$, $\mathbf{A}^{\mathrm{T}}$, and $\mathbf{A}^{\mathrm{H}}$ denotes conjugate, transpose and conjugate transpose, respectively. $\mathcal{CN}(0, \sigma^2)$ denotes a circularly symmetric complex Gaussian random variable with zero mean and variance σ^2. The identity matrix of size K is denoted by $\mathbf{I}_K$. $(\cdot)_{\mathrm{R}}$ and $(\cdot)_{\mathrm{I}}$ denote the real and imaginary parts, respectively. For a complex number a, $|a|$ and $\angle a$ denotes the absolute value and the angle of a. The operation

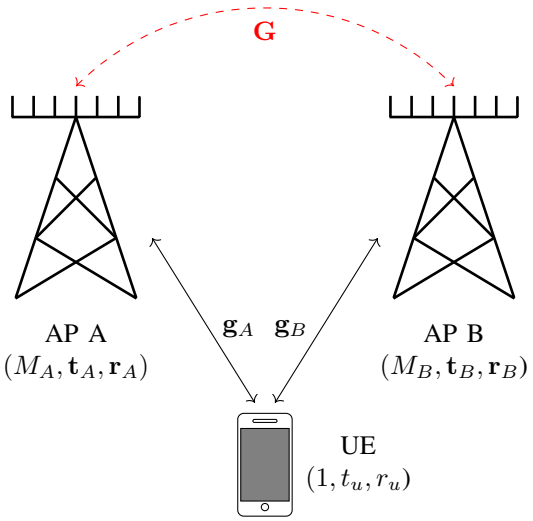

Fig. 1: A distributed massive MIMO system with two APs serving a UE. The triple $(\cdot,\cdot,\cdot)$ refers to (number of antennas, transmit chain gains, receive chain gains) at each unit.

$\mathrm{vec}(\cdot)$ denotes vectorization. The notations $\|\cdot\|_{\mathrm{F}}$ and $\|\cdot\|_2$ denote the Frobenius and l_2 norms, respectively.

II. System Model

Consider two multi-antenna APs A and B, equipped with M_A and M_B antennas, respectively, serving a single antenna UE as shown in Fig. 1. Each antenna at the AP has a dedicated RF chain and all the RF chains in a given AP are driven by a single LO. Let $\mathbf{G} \in \mathbb{C}^{M_A \times M_B}$ be the reciprocal channel between A and B. Let $\mathbf{t}_A = \begin{bmatrix} t_1^A & t_2^A & \cdots & t_{M_A}^A \end{bmatrix}^{\mathrm{T}}$, and $\mathbf{r}_A = \begin{bmatrix} r_1^A & r_2^A & \cdots & r_{M_A}^A \end{bmatrix}^{\mathrm{T}}$ be the transmit and receive gains at all the RF chains of AP A. Similarly let $\mathbf{t}_B = \begin{bmatrix} t_1^B & t_2^B & \cdots & t_{M_B}^B \end{bmatrix}^{\mathrm{T}}$ and $\mathbf{r}_B = \begin{bmatrix} r_1^B & r_2^B & \cdots & r_{M_B}^B \end{bmatrix}^{\mathrm{T}}$ be the transmit and receive gains at all the RF chains of AP B. We assume that both APs are individually reciprocity calibrated according to [11]. For clarity reciprocity calibration of a multi-antenna AP is presented in the Appendix. During the transmission, each AP multiplies with the internal calibration coefficient corresponding to each of the antennas. For example, for the mth antenna at AP A, during the transmission of the signal, the calibration coefficient $\frac{t_1^A r_m^A}{r_1^A t_m^A}$ will be multiplied with. This ensures that both the APs are reciprocity calibrated to their first antenna. For the coherent combining of signals from APs A and B, we require a phase calibration between the two APs. Mathematically, we need to estimate the phase offset $(\angle t_1^A - \angle r_1^A) - (\angle t_1^B - \angle r_1^B)$ between the APs and correct it during the downlink transmission to the UE.

III. BeamSync: Phase Synchronization

We propose an over-the-air synchronization procedure, BeamSync, to phase calibrate the reciprocity-calibrated APs. We sent an omnidirectional pilot signal from AP A, from which AP B estimates the dominant direction of the reception of the signal. Then, AP B beamforms the phase synchronization signal to AP A in the dominant direction between the two APs. AP A sends back this signal to AP B for the estimation of phase offset. BeamSync is a fully digital synchronization technique, and hence, we can beamform the signals in any 3-dimensional direction. Let $\varphi_A = \angle t_1^A - \angle r_1^A$ and $\varphi_B = \angle t_1^B - \angle r_1^B$ and $\varphi = \varphi_A - \varphi_B$. Our proposed over-the-air phase synchronization protocol between two APs consists of three stages as follows:

Stage-I: Let $\mathbf{\Phi} = \begin{bmatrix} \phi_1, \phi_2, \cdots, \phi_{M_A} \end{bmatrix} \in \mathbb{C}^{L \times M_A}$ be a pilot matrix at AP A such that $\mathbf{\Phi}^{\mathrm{H}}\mathbf{\Phi} = \mathbf{I}_{M_A}$ and $L \geq M_A$ is the pilot signal length. In the first stage, AP A sends the pilot matrix $\mathbf{\Phi}$ and the received signal at AP B, $\mathbf{Y}_{B1} \in \mathbb{C}^{M_B \times L}$ is given by

$$\begin{aligned} \mathbf{Y}_{B1} &= \frac{t_1^A}{r_1^A} \mathbf{D}_{\mathbf{r}_B} \mathbf{G}^{\mathrm{T}} \mathbf{D}_{\mathbf{r}_A} \mathbf{\Phi}^{\mathrm{T}} + \mathbf{W}_{B1} \\ &= \frac{t_1^A}{r_1^A} \mathbf{G}_e^{\mathrm{T}} \mathbf{\Phi}^{\mathrm{T}} + \mathbf{W}_{B1}, \end{aligned} \tag{1}$$

where $\mathbf{G}_e = \mathbf{D}_{\mathbf{r}_A} \mathbf{G} \mathbf{D}_{\mathbf{r}_B}$ is the effective channel matrix and $\mathbf{W}_{B1}$ is additive white Gaussian noise (AWGN) with independent and identically distributed (i.i.d.) $\mathcal{CN}(0, \sigma^2)$ entries with σ^2 as the noise power. The notation $\mathbf{D}_{\mathbf{a}}$ denotes a diagonal matrix with the elements of the vector $\mathbf{a}$ as diagonal entries.

Stage-II: AP B determines a unitary beamforming vector $\mathbf{a} \in \mathbb{C}^{M_B \times 1}$ from the received signal $\mathbf{Y}_{B1}$. Let $\mathbf{x} \in \mathbb{C}^{N \times 1}$ be phase synchronization signal such that $\|\mathbf{x}\|^2 = N$. In the second stage, AP B beamforms $\mathbf{x}$ in the direction $\mathbf{a}$. The signal received at AP A , $\mathbf{Y}_{A1} \in \mathbb{C}^{M_A \times N}$ can be written as

$$\mathbf{Y}_{A1} = \frac{t_1^B}{r_1^B} \mathbf{G}_e \mathbf{a} \mathbf{x}^{\mathrm{T}} + \mathbf{W}_{A1}, \tag{2}$$

where $\mathbf{W}_{A1}$ is AWGN with i.i.d. $\mathcal{CN}(0, \sigma^2)$ entries.

Stage-III: Let

$$c = \frac{N}{\|\mathbf{Y}_{A1}\|_F^2}. \tag{3}$$

In the third stage, AP A transmits a scaled version of the conjugate of the signal received during the second stage to AP B. The received signal at AP B, $\mathbf{Y}_{B2} \in \mathbb{C}^{M_B \times N}$ can be written as

$$\begin{aligned} \mathbf{Y}_{B2} &= \sqrt{c} \frac{t_1^A}{r_1^A} \mathbf{G}_e^{\mathrm{T}} \mathbf{Y}_{A1}^* + \mathbf{W}_{B2} \\ &= \sqrt{c} \frac{t_1^A}{r_1^A} \mathbf{G}_e^{\mathrm{T}} \left(\frac{t_1^B}{r_1^B} \mathbf{G}_e \mathbf{a} \mathbf{x}^{\mathrm{T}} + \mathbf{W}_{A1} \right)^* + \mathbf{W}_{B2}, \end{aligned} \tag{4}$$

where $\mathbf{W}_{B2}$ is AWGN with i.i.d. $\mathcal{CN}(0, \sigma^2)$ entries.

A. Phase Offset Estimation

Let

$$\begin{aligned} c_1 &= \sqrt{c} \frac{|t_1^A|\,|t_1^B|}{|r_1^A|\,|r_1^B|} \\ c_2 &= \sqrt{c} \frac{|t_1^A|}{|r_1^A|}. \end{aligned} \tag{5}$$

Then (4) can we written as

$$\begin{aligned} \mathbf{Y}_{B2} &= e^{j\varphi} c_1 \mathbf{G}_e^{\mathrm{T}} \mathbf{G}_e^* \mathbf{a}^* \mathbf{x}^{\mathrm{H}} + e^{j\varphi_A} c_2 \mathbf{G}_e^{\mathrm{T}} \mathbf{W}_{A1}^* + \mathbf{W}_{B2} \\ &= e^{j\varphi} c_1 \mathbf{G}_e^{\mathrm{T}} \mathbf{G}_e^* \mathbf{a}^* \mathbf{x}^{\mathrm{H}} + \mathbf{W}', \end{aligned} \tag{6}$$

where $\mathbf{W}' = e^{j\varphi_A} c_2 \mathbf{G}_e^{\mathrm{T}} \mathbf{W}_{A1}^* + \mathbf{W}_{B2}$. Conditioned on $\mathbf{G}$ and c_2, each column of $\mathbf{W}'$ is distributed as $\mathcal{CN}(0, \left(\mathbf{I} + c_2^2 \mathbf{G}_e^{\mathrm{T}} \mathbf{G}_e^*\right) \sigma^2)$. Let

$$\begin{aligned} \mathbf{Z} &= c_1 \mathbf{G}_e^{\mathrm{T}} \mathbf{G}_e^* \mathbf{a}^* \mathbf{x}^{\mathrm{H}} \\ \mathbf{R} &= \mathbf{I} + c_2^2 \mathbf{G}_e^{\mathrm{T}} \mathbf{G}_e^*. \end{aligned} \tag{7}$$

Then $\mathbf{Y}_{B2} = e^{j\varphi}\mathbf{Z} + \mathbf{W}'$. Using NLS estimation, the estimate of φ is given by

$$\begin{aligned} \hat{\varphi} &= \underset{\varphi}{\operatorname{argmin}} \operatorname{Tr}\left\{ \left(\mathbf{Y}_{B2} - e^{j\varphi}\mathbf{Z}\right)^{\mathrm{H}} \mathbf{R}^{-1} \left(\mathbf{Y}_{B2} - e^{j\varphi}\mathbf{Z}\right) \right\} \\ &= \underset{\varphi}{\operatorname{argmin}} \operatorname{Tr}\left\{ \mathbf{R}^{-\frac{1}{2}} \left(\mathbf{Y}_{B2} - e^{j\varphi}\mathbf{Z}\right) \left(\mathbf{Y}_{B2} - e^{j\varphi}\mathbf{Z}\right)^{\mathrm{H}} \mathbf{R}^{-\frac{1}{2}} \right\} \\ &= \underset{\varphi}{\operatorname{argmin}} \left\| \mathbf{R}^{-\frac{1}{2}} \mathbf{Y}_{B2} - e^{j\varphi} \mathbf{R}^{-\frac{1}{2}} \mathbf{Z} \right\|_{\mathrm{F}}^2 \\ &= \underset{\varphi}{\operatorname{argmin}} \left\| \operatorname{vec}\left(\mathbf{R}^{-\frac{1}{2}} \mathbf{Y}_{B2}\right) - e^{j\varphi} \operatorname{vec}\left(\mathbf{R}^{-\frac{1}{2}} \mathbf{Z}\right) \right\|_2^2. \end{aligned} \tag{8}$$

From (8), the estimate of φ is the angle between the two vectors $\operatorname{vec}\left(\mathbf{R}^{-\frac{1}{2}} \mathbf{Y}_{B2}\right)$ and $\operatorname{vec}\left(\mathbf{R}^{-\frac{1}{2}} \mathbf{Z}\right)$. Mathematically,

$$\begin{aligned} \hat{\varphi} &= \angle \left(\operatorname{vec}\left(\mathbf{R}^{-\frac{1}{2}} \mathbf{Z}\right)^{\mathrm{H}} \operatorname{vec}\left(\mathbf{R}^{-\frac{1}{2}} \mathbf{Y}_{B2}\right) \right) \\ &= \angle \left(\operatorname{Tr}\left\{ \mathbf{Z}^{\mathrm{H}} \mathbf{R}^{-1} \mathbf{Y}_{B2} \right\} \right) \\ &= \angle \left(\operatorname{Tr}\left\{ c_1 \mathbf{x} \mathbf{a}^{\mathrm{T}} \mathbf{G}_e^{\mathrm{T}} \mathbf{G}_e^* \mathbf{R}^{-1} \mathbf{Y}_{B2} \right\} \right) \\ &= \angle \left(\mathbf{a}^{\mathrm{T}} \mathbf{G}_e^{\mathrm{T}} \mathbf{G}_e^* \mathbf{R}^{-1} \mathbf{Y}_{B2} \mathbf{x} \right) \\ &= \angle \left(\mathbf{a}^{\mathrm{T}} \mathbf{G}_e^{\mathrm{T}} \mathbf{G}_e^* \left(\mathbf{I} + c_2^2 \mathbf{G}_e^{\mathrm{T}} \mathbf{G}_e^*\right)^{-1} \mathbf{Y}_{B2} \mathbf{x} \right). \end{aligned} \tag{9}$$

The complexity of the NLS estimator is $\mathcal{O}(M_B^3)$ due to the matrix inversion term. Thus, as the number of antennas in the AP increases the complexity also increases. However, if the SNR is high at stage-III, we can approximate $\mathbf{R}$ as $c_2^2 \mathbf{G}_e^{\mathrm{T}} \mathbf{G}_e^*$, which is possible in practice as the APs are not power limited. Thus, the estimate for φ at high SNR is given by

$$\hat{\varphi} = \angle \left(\mathbf{a}^{\mathrm{T}} \mathbf{Y}_{B2} \mathbf{x} \right). \tag{10}$$

The simple sub-optimal estimator in (10) performs the same as NLS estimator at high SNR with significantly lower complexity, and requiring only matrix multiplications.

B. Optimal Beamforming Direction

Let

$$b = \left\| \left(\mathbf{I} + c_2^2 \mathbf{G}_e^{\mathrm{T}} \mathbf{G}_e^*\right)^{-\frac{1}{2}} \mathbf{G}_e^{\mathrm{T}} \mathbf{G}_e^* \mathbf{a}^* \right\|_2^2. \tag{11}$$

Consider the test statistic in (9)

$$\begin{aligned} y_B &= \mathbf{a}^{\mathrm{T}} \mathbf{G}_e^{\mathrm{T}} \mathbf{G}_e^* \left(\mathbf{I} + c_2^2 \mathbf{G}_e^{\mathrm{T}} \mathbf{G}_e^*\right)^{-1} \mathbf{Y}_{B2} \mathbf{x} \\ &= \mathbf{a}^{\mathrm{T}} \mathbf{G}_e^{\mathrm{T}} \mathbf{G}_e^* \left(\mathbf{I} + c_2^2 \mathbf{G}_e^{\mathrm{T}} \mathbf{G}_e^*\right)^{-1} (e^{j\varphi} c_1 \mathbf{G}_e^{\mathrm{T}} \mathbf{G}_e^* \mathbf{a}^* \mathbf{x}^{\mathrm{H}} + \mathbf{W}') \mathbf{x} \\ &= e^{j\varphi} c_1 b \left\|\mathbf{x}\right\|_2^2 + w \\ &= e^{j\varphi} c_1 N b + w, \end{aligned} \tag{12}$$

where $w = \mathbf{a}^{\mathrm{T}} \mathbf{G}_e^{\mathrm{T}} \mathbf{G}_e^* \left(\mathbf{I} + c_2^2 \mathbf{G}_e^{\mathrm{T}} \mathbf{G}_e^*\right)^{-1} \mathbf{W}' \mathbf{x}$. In (12), the columns of the matrix $\mathbf{W}'$ are colored with covariance $\mathbf{R}$. Hence, the noise power depends on the choice of phase synchronization signal $\mathbf{x}$. From (12), the estimation error in φ can be reduced by increasing the synchronization signal length N as well as by maximizing the value of b. Specifically, the SNR in (12) is proportional to both N and b. In this subsection, we find the optimal beamforming direction $\mathbf{a}$ that maximizes b.

Let the singular value decomposition (SVD) of the effective channel $\mathbf{G}_e$ be

$$\mathbf{G}_e = \mathbf{U} \mathbf{\Sigma} \mathbf{V}^{\mathrm{H}}, \tag{13}$$

where $\mathbf{U} \in \mathbb{C}^{M_A \times M_A}$ and $\mathbf{V} \in \mathbb{C}^{M_B \times M_B}$ are unitary matrices and $\mathbf{\Sigma} \in \mathbb{R}^{M_A \times M_B}$ with singular values of $\mathbf{G}_e$ in decreasing order on its principal diagonal. Then, we have

$$\mathbf{G}_e^{\mathrm{T}} \mathbf{G}_e^* = \mathbf{V}^* \mathbf{\Lambda} \mathbf{V}^{\mathrm{T}}, \tag{14}$$

where $\mathbf{\Lambda} = \mathbf{\Sigma}^{\mathrm{T}} \mathbf{\Sigma} \in \mathbb{R}^{M_B \times M_B}$ is a diagonal matrix. Let $\lambda_1 \geq \lambda_2 \geq \cdots \geq \lambda_{M_B}$ be the diagonal elements of $\mathbf{\Lambda}$ in decreasing order. Substituting (14) for b, we have

$$\begin{aligned} b &= \mathbf{a}^{\mathrm{T}} \mathbf{G}_e^{\mathrm{T}} \mathbf{G}_e^* \left(\mathbf{I} + c_2^2 \mathbf{G}_e^{\mathrm{T}} \mathbf{G}_e^*\right)^{-1} \mathbf{G}_e^{\mathrm{T}} \mathbf{G}_e^* \mathbf{a}^* \\ &= \mathbf{a}^{\mathrm{T}} \mathbf{V}^* \mathbf{\Lambda} \mathbf{V}^{\mathrm{T}} \left(\mathbf{V}^* \mathbf{V}^{\mathrm{T}} + c_2^2 \mathbf{V}^* \mathbf{\Lambda} \mathbf{V}^{\mathrm{T}}\right)^{-1} \mathbf{V}^* \mathbf{\Lambda} \mathbf{V}^{\mathrm{T}} \mathbf{a}^* \\ &= \mathbf{a}^{\mathrm{T}} \mathbf{V}^* \mathbf{\Lambda} \left(\mathbf{I} + c_2^2 \mathbf{\Lambda}\right)^{-1} \mathbf{\Lambda} \mathbf{V}^{\mathrm{T}} \mathbf{a}^* \\ &= \mathbf{a}^{\mathrm{T}} \mathbf{V}^* \mathbf{\Lambda}' \mathbf{V}^{\mathrm{T}} \mathbf{a}^*, \end{aligned} \tag{15}$$

where $\mathbf{\Lambda}' = \mathbf{\Lambda} \left(\mathbf{I} + c_2^2 \mathbf{\Lambda}\right)^{-1} \mathbf{\Lambda}$ is a diagonal matrix. Consider the difference between the first and the second diagonal elements of $\mathbf{\Lambda}'$, i.e.,

$$\begin{aligned} \frac{\lambda_1^2}{1 + c_2^2 \lambda_1} - \frac{\lambda_2^2}{1 + c_2^2 \lambda_2} &= \frac{(\lambda_1 - \lambda_2)(\lambda_1 + \lambda_2 + c_2^2 \lambda_1 \lambda_2)}{(1 + c_2^2 \lambda_1)(1 + c_2^2 \lambda_2)} \\ &\geq 0. \end{aligned} \tag{16}$$

Thus, the diagonal entries of $\mathbf{\Lambda}'$ is also in the decreasing order. The value of b can be maximized by choosing $\mathbf{a} = \mathbf{v}_1$, where the vector $\mathbf{v}_1$ is the first column of the matrix $\mathbf{V}$, which corresponds to the dominant direction of the effective channel in which the signal was received at AP B from AP A. Thus, by beamforming the synchronization signal $\mathbf{x}$ in the dominant direction of the effective channel, a better estimate of the phase offset φ could be obtained.

Consider the test statistic in (9) and when we beamform the synchronization signal in the optimal direction, the statistic can be further reduced as follows:

$$\begin{aligned} \hat{\varphi} &= \angle \left(\mathbf{a}^{\mathrm{T}} \mathbf{G}_e^{\mathrm{T}} \mathbf{G}_e^* \left(\mathbf{I} + c_2^2 \mathbf{G}_e^{\mathrm{T}} \mathbf{G}_e^*\right)^{-1} \mathbf{Y}_{B2} \mathbf{x} \right) \\ &= \angle \left(\mathbf{v}_1^{\mathrm{T}} \mathbf{V}^* \mathbf{\Lambda} \mathbf{V}^{\mathrm{T}} \left(\mathbf{V}^* \mathbf{V}^{\mathrm{T}} + c_2^2 \mathbf{V}^* \mathbf{\Lambda} \mathbf{V}^{\mathrm{T}}\right)^{-1} \mathbf{Y}_{B2} \mathbf{x} \right) \\ &= \angle \left(\frac{\lambda_1}{1 + c_2^2 \lambda_1} \mathbf{v}_1^{\mathrm{T}} \mathbf{Y}_{B2} \mathbf{x} \right) \\ &= \angle \left(\mathbf{v}_1^{\mathrm{T}} \mathbf{Y}_{B2} \mathbf{x} \right). \end{aligned} \tag{17}$$

Thus, if we beamform in the optimal direction, the optimal test statistic in (9) becomes same as the simpler test statistic in (10).

C. Estimating the Beamforming Direction

From Sec. III-B, it is evident that the optimal direction to beamform is the dominant direction of the effective channel in which AP B receives the signal from the AP A. In practice, the effective channel $\mathbf{G}_e$ is not perfectly known at either APs.

Algorithm 1: Phase Synchronization Algorithm

1: Transmit omnidirectional pilot signal $\mathbf{\Phi}$ from AP A
2: Compute the SVD of the received signal $\mathbf{Y}_{B1} = \mathbf{U}_B\mathbf{\Sigma}_B\mathbf{V}_B^{\mathrm{H}}$ at AP B
3: AP B sends the phase synchronization signal $\mathbf{x}$ by beamforming in the direction $\mathbf{a} = \mathbf{u}_{B1}^{*}$
4: AP A transmits the conjugate of the received signal back to AP B
5: AP B estimates the phase difference $\varphi = \angle\left(\mathbf{a}^{\mathrm{T}}\mathbf{Y}_{B2}\mathbf{x}\right)$ and precompensates its phase during transmission.

However, as the effective channel is reciprocal, the AP B can estimate the dominant direction from the signal received in stage-I, without the need to estimate the effective channel, by computing the SVD of the received signal $\mathbf{Y}_{B1}$. Let

$$\mathbf{Y}_{B1} = \mathbf{U}_B\mathbf{\Sigma}_B\mathbf{V}_B^{\mathrm{H}}, \tag{18}$$

where $\mathbf{U}_B \in \mathbb{C}^{M_B\times M_B}$ and $\mathbf{V}_B \in \mathbb{C}^{L\times L}$ are unitary matrices and $\mathbf{\Sigma}_B \in \mathbb{R}^{M_B\times L}$ is a diagonal matrix with the singular values of $\mathbf{Y}_{B1}$ in decreasing order. The dominant direction in which the signal is received is $\mathbf{u}_{B1}$, where $\mathbf{u}_{B1}$ is the first column of $\mathbf{U}_B$. Thus, the beamforming direction is chosen as $\mathbf{a} = \mathbf{u}_{B1}^{*}$. The BeamSync protocol to synchronize the phase difference between APs A and B is provided in algorithm 1. In terms of computational complexity, the algorithm consists of linear operations plus a computation of the dominant eigenvector of a matrix. The dominant eigenvector can be computed by a variety of algorithms, for example, a power iteration [33].

D. Phase Synchronization Among Multiple APs

In this section, we consider how to extend the BeamSync phase synchronization algorithm to the case of multiple APs. To synchronize the APs to a common reference, we nominate one of the APs as the master AP and the remaining APs as slave APs. Let there be K slave APs in the network. Let $\mathbf{G}_k$ be the channel between the master AP and the kth slave AP. The BeamSync protocol for phase synchronization among multiple APs is illustrated in Fig. 2. The stage-I pilot signal is broadcast from the master AP to all slave APs and all the slave APs estimates its dominant direction of the signal received from the master AP. Note that, the pilot signal from the master needs to be sent only once during the entire synchronization. Afterward, sequentially or multiplexed in frequency, to avoid interference, each slave AP sends the phase synchronization signal to the master AP (stage-II) and the master sends back the conjugate of the received signal (stage-III) to each of the APs for estimation of the phase offset. The frequency subbands and timeslots will not be orthogonal until the system is completely synchronized. For synchronization purposes, guard bands in time and frequency need to be inserted to avoid interference due to non-orthogonality.

The synchronization scheme in [32] requires all the participating APs to sequentially transmit beams in all directions and listen to others. This requires a large number of measurements

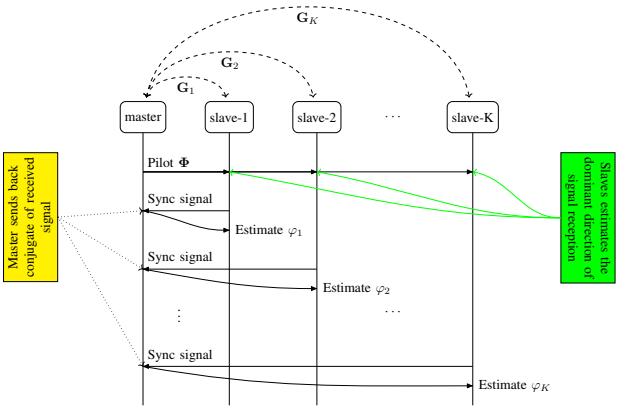

Fig. 2: BeamSync protocol for phase synchronization.

to be carried out. Considering M antennas per each AP, the total number of measurements required is $(K+1)M^2$ and all these measurements need to be sent to the CPU for joint estimation of the phase offsets, which requires additional fronthaul signaling. However, with BeamSync, the master AP needs to send the pilot signal once, which requires only L measurements. The slave APs then estimate the dominant direction of the received signal and carry out the synchronization procedure using stage-II and III sequentially, requiring a total of $2N$ measurements for each master-slave pair and hence, a total of $2KN$ measurements.

IV. BeamSync: Frequency Synchronization

In this section, we discuss how BeamSync can be used for synchronizing the carrier frequency between two reciprocity-calibrated APs. As the local oscillators driving the RF chain of the different base station differs, there exists a carrier frequency offset between the base stations. Let $\Delta \in \mathbb{R}$ be the frequency offset between A and B.

A. BeamSync for Frequency Synchronization

The protocol consists of two stages described as follows:

Stage-I: AP B transmits an orthonormal pilot sequence of length $L_B \geq M_B$ from each of its antennas. Let the columns of the matrix $\mathbf{\Phi}_{\mathrm{B}} \in \mathbb{C}^{L_B\times M_B}$, where $\mathbf{\Phi}_{\mathrm{B}}^{\mathrm{H}}\mathbf{\Phi}_{\mathrm{B}} = \mathbf{I}_{M_B}$, denote the set of orthonormal pilot sequences. Let

$$\mathbf{\Delta}_\tau = \left[e^{j2\pi\Delta T}\ e^{j2\pi 2\Delta T}\ \cdots\ e^{j2\pi\tau\Delta T}\right]^{\mathrm{T}} \in \mathbb{C}^{\tau\times 1}, \tag{19}$$

where T is the symbol arrival time. The collective signal received in L_B time instants at AP A, $\mathbf{Y}_A \in \mathbb{C}^{M_A\times L_B}$ can be written as

$$\mathbf{Y}_A = \frac{t_1^B}{r_1^B}\mathbf{G}_e\mathbf{\Phi}_{\mathrm{B}}^{\mathrm{T}}\mathbf{D}_{\mathbf{\Delta}_{L_B}} + \mathbf{W}_A, \tag{20}$$

where $\mathbf{W}_A \in \mathbb{C}^{M_A\times L_B}$ is AWGN with i.i.d. $\mathcal{CN}(0,\sigma^2)$ entries.

Stage-II: AP A processes the signal $\mathbf{Y}_A$ received in stage-I and determines a unitary beamforming vector $\mathbf{a}_{\mathrm{f}} \in \mathbb{C}^{M_A\times 1}$. It then beamforms an N_f-length frequency synchronization

signal $\mathbf{x}_\mathrm{f}$ towards AP B. Moreover, we assume that $\mathbf{x}_\mathrm{f}$ is real-valued. The received signal at AP B, $\mathbf{Y}_B \in \mathbb{C}^{M_B \times N_f}$ can be written as

$$\mathbf{Y}_B = \frac{t_1^A}{r_1^A}\mathbf{G}_e^\mathrm{T}\mathbf{a}_\mathrm{f}\mathbf{x}_\mathrm{f}^\mathrm{T}\mathbf{D}^*_{\mathbf{\Delta}_{N_f}} + \mathbf{W}_B, \tag{21}$$

where $\mathbf{W}_B \in \mathbb{C}^{M_B \times N_f}$ is AWGN with i.i.d. $\mathcal{CN}(0,\sigma^2)$ entries. AP B needs to estimate its frequency offset Δ with respect to AP A from (21). Let

$$\mathbf{b} = \frac{t_1^A}{r_1^A}\mathbf{G}_e^\mathrm{T}\mathbf{a}_\mathrm{f}. \tag{22}$$

Then (21) can be rewritten as

$$\mathbf{Y}_B = \mathbf{b}\mathbf{x}_\mathrm{f}^\mathrm{T}\mathbf{D}^*_{\mathbf{\Delta}_{N_f}} + \mathbf{W}_B. \tag{23}$$

The joint maximum-likelihood estimates of $\mathbf{b}$ and Δ are given by

$$(\hat{\mathbf{b}},\hat{\Delta}) = \underset{\mathbf{b},\Delta}{\operatorname{argmin}} \|\mathbf{Y}_B - \mathbf{b}\mathbf{x}_\mathrm{f}^\mathrm{T}\mathbf{D}^*_{\mathbf{\Delta}_{N_f}}\|^2. \tag{24}$$

Solving (24) using NLS estimation in Gaussian noise [34, Sec. 8.9] with $\mathbf{b}$ as a nuisance parameter, the estimates of $\mathbf{b}$ and Δ are given by

$$\hat{\mathbf{b}} = \frac{\mathbf{Y}_B\mathbf{D}_{\mathbf{\Delta}_{N_f}}\mathbf{x}_\mathrm{f}}{\|\mathbf{x}_\mathrm{f}\|^2} \tag{25}$$

$$\hat{\Delta} = \underset{\Delta}{\operatorname{argmax}} \|\mathbf{Y}_B\mathbf{D}_{\mathbf{\Delta}_{N_f}}\mathbf{x}_\mathrm{f}\|^2. \tag{26}$$

In the next subsection, we discuss the optimal beamforming direction and the parameters affecting the frequency offset estimation performance.

B. Optimal Beamforming Direction

Here, we derive the optimal beamforming direction that minimizes the frequency offset estimation error. We look at the conditions for which the Cramér-Rao lower bound (CRB) on the estimate of Δ, is minimized. We have $\mathbf{b} = \mathbf{b}_\mathrm{R} + j\mathbf{b}_\mathrm{I}$. Let

$$\boldsymbol{\theta} = [\mathbf{b}_\mathrm{R}^\mathrm{T}\ \mathbf{b}_\mathrm{I}^\mathrm{T}\ \Delta]^\mathrm{T} \tag{27}$$

be the unknown vector parameter at AP B. From (23), the signal received at the n^{th} time instant, $\mathbf{y}_B(n) \in \mathbb{C}^{M_B\times 1}$ is given by

$$\mathbf{y}_B(n) = \mathbf{b}x_\mathrm{f}(n)e^{-j2\pi n\Delta} + \mathbf{w}_B(n), \tag{28}$$

where $x_\mathrm{f}(n)$ is the nth component of $\mathbf{x}_\mathrm{f}$ and $\mathbf{w}_B(n)$ is the nth column of $\mathbf{W}_B$. Also $\mathbf{y}_B(n)$ is distributed as $\mathcal{CN}(\mathbf{b}x_\mathrm{f}(n)e^{-j2\pi n\Delta}, \sigma^2\mathbf{I}_{M_B})$. Let $\mathbf{y}_{B\mathrm{R}}(n)$ and $\mathbf{y}_{B\mathrm{I}}(n)$ be the real and imaginary parts of $\mathbf{y}_B(n)$. Thus, $\bar{\mathbf{y}}_B(n) = [\mathbf{y}_{B\mathrm{R}}^\mathrm{T}(n)\ \mathbf{y}_{B\mathrm{I}}^\mathrm{T}(n)]^\mathrm{T} \in \mathbb{R}^{2M_B\times 1}$ is distributed as $\mathcal{N}(\boldsymbol{\mu}_n(\boldsymbol{\theta}), \mathbf{C}(\boldsymbol{\theta}))$, where $\boldsymbol{\mu}_n$ and $\mathbf{C}$ are mean vector and covariance matrix, respectively, of $\bar{\mathbf{y}}_B$ parameterized by $\boldsymbol{\theta}$, and are given by

$$\boldsymbol{\mu}_n(\boldsymbol{\theta}) = x_\mathrm{f}(n)\begin{bmatrix}\mathbf{b}_\mathrm{R}\cos(2\pi n\Delta) + \mathbf{b}_\mathrm{I}\sin(2\pi n\Delta)\\ -\mathbf{b}_\mathrm{R}\sin(2\pi n\Delta) + \mathbf{b}_\mathrm{I}\cos(2\pi n\Delta)\end{bmatrix} \tag{29}$$

$$\mathbf{C}(\boldsymbol{\theta}) = \frac{\sigma^2}{2}\mathbf{I}_{2M_B}. \tag{30}$$

Using the Slepian Bang theorem [34, Sec. 3.9], each element of the Fisher information matrix (FIM) of $\boldsymbol{\theta}$ at n^{th} time instant, $\mathbf{J}_n(\boldsymbol{\theta}) \in \mathbb{R}^{(2M_B+1)\times(2M_B+1)}$, can be computed as

$$\begin{aligned}[\mathbf{J}_n(\boldsymbol{\theta})]_{k,l} = &\left[\frac{\partial\boldsymbol{\mu}_n(\boldsymbol{\theta})}{\partial\boldsymbol{\theta}_k}\right]^\mathrm{T}\mathbf{C}^{-1}(\boldsymbol{\theta})\left[\frac{\partial\boldsymbol{\mu}_n(\boldsymbol{\theta})}{\partial\boldsymbol{\theta}_l}\right]\\ &+\frac{1}{2}\operatorname{Tr}\left[\mathbf{C}^{-1}(\boldsymbol{\theta})\frac{\partial\mathbf{C}(\boldsymbol{\theta})}{\partial\boldsymbol{\theta}_k}\mathbf{C}^{-1}(\boldsymbol{\theta})\frac{\partial\mathbf{C}(\boldsymbol{\theta})}{\partial\boldsymbol{\theta}_l}\right].\end{aligned} \tag{31}$$

By computing the partial derivatives of (29) and (30), we obtain

$$\mathbf{J}_n(\boldsymbol{\theta}) = \frac{2x_\mathrm{f}^2(n)}{\sigma^2}\begin{bmatrix}\mathbf{I}_{M_B} & \mathbf{0} & 2\pi n\mathbf{b}_\mathrm{I}\\ \mathbf{0} & \mathbf{I}_{M_B} & -2\pi n\mathbf{b}_\mathrm{R}\\ 2\pi n\mathbf{b}_\mathrm{I}^\mathrm{T} & -2\pi n\mathbf{b}_\mathrm{R}^\mathrm{T} & 4\pi^2n^2\|\mathbf{b}\|^2\end{bmatrix}. \tag{32}$$

The received signal $\mathbf{y}_B(n)$ is independent for different time instants. Thus, using the additive property of FIM, the overall FIM of $\boldsymbol{\theta}$, $\mathbf{J}(\boldsymbol{\theta})$, is given by

$$\mathbf{J}(\boldsymbol{\theta}) = \sum_{n=1}^{N_f}\mathbf{J}_n(\boldsymbol{\theta}). \tag{33}$$

The CRB of $\hat{\Delta}$ can be computed from $\mathrm{J}(\boldsymbol{\theta})$ as

$$\mathrm{CRB}(\hat{\Delta}) = \left[\mathbf{J}^{-1}(\boldsymbol{\theta})\right]_{2M_B+1,2M_B+1}, \tag{34}$$

which is the lower right corner element of $\mathbf{J}^{-1}(\boldsymbol{\theta})$. Using the inverse of a block partitioned matrix [35, Sec. 0.7.3], the CRB of $\hat{\Delta}$ is given by

$$\mathrm{CRB}(\hat{\Delta}) = \frac{\sigma^2}{8\pi^2\|\mathbf{b}\|^2\left(\sum_{n=1}^{N_f}n^2x_\mathrm{f}^2(n) - \frac{(\sum_{n=1}^{N_f}nx_\mathrm{f}^2(n))^2}{\sum_{n=1}^{N_f}x_\mathrm{f}^2(n)}\right)}. \tag{35}$$

From (35), the CRB of $\hat{\Delta}$ will be minimized when

$$\|\mathbf{b}\|^2 = \left(\frac{|t_1^A|}{|r_1^A|}\right)^2\left\|\mathbf{G}_e^\mathrm{T}\mathbf{a}_\mathrm{f}\right\|^2 \tag{36}$$

is maximized. From (13), we have

$$\left\|\mathbf{G}_e^\mathrm{T}\mathbf{a}_\mathrm{f}\right\|^2 = \mathbf{a}_\mathrm{f}^\mathrm{H}\mathbf{U}^*\mathbf{\Sigma}\mathbf{\Sigma}^\mathrm{T}\mathbf{U}^\mathrm{T}\mathbf{a}_\mathrm{f}, \tag{37}$$

and can be maximized by choosing $\mathbf{a}_\mathrm{f} = \mathbf{u}_1^*$. The vector $\mathbf{u}_1$, is the first column of matrix $\mathbf{U}$. Hence, the optimal beamforming direction $\mathbf{a}_\mathrm{f}$ corresponds to the dominant direction of the effective channel in which the signal is received at AP A from AP B. Similar to the phase synchronization, the beamforming vector can be obtained by AP A from $\mathbf{Y}_A$. Let the SVD of $\mathbf{Y}_A$ be

$$\mathbf{Y}_A = \mathbf{U}_A\mathbf{\Sigma}_A\mathbf{V}_A^\mathrm{H}. \tag{38}$$

Then the beamforming vector is chosen as $\mathbf{a}_\mathrm{f} = \mathbf{u}_{A1}^*$, where $\mathbf{u}_{A1}$ is the first column of matrix $\mathbf{U}_A$.

From (35), for estimating Δ, the synchronization signal length N_f should be at least 2. Also, as N_f increases, the denominator in (35) increases. Thus, increasing the synchronization sequence length N_f improves the estimation quality. Moreover, the CRB of the estimate of Δ can be reduced by increasing the SNR, which in turn improves the estimation quality. The frequency synchronization algorithm is provided in algorithm 2.

Algorithm 2: Frequency Synchronization Algorithm

1: Transmit omnidirectional pilot signal $\mathbf{\Phi}_{\mathrm{B}}$ from AP B
2: Compute SVD of received signal $\mathbf{Y}_A = \mathbf{U}_A \mathbf{\Sigma}_A \mathbf{V}_A^{\mathrm{H}}$ at AP A
3: AP A sends the frequency synchronization signal $\mathbf{x}_{\mathrm{f}}$ by beamforming in the direction $\mathbf{a}_{\mathrm{f}} = \mathbf{u}_{A1}^{*}$
4: AP B estimates the carrier frequency offset $\hat{\Delta}$ and precompensate its frequency during transmission.

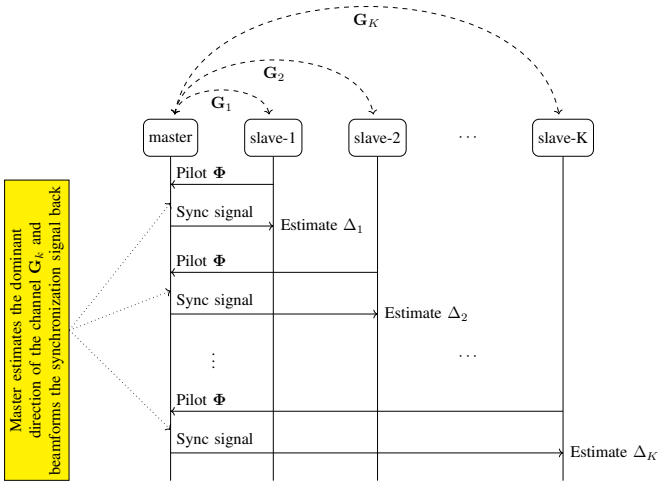

Fig. 3: BeamSync protocol for frequency synchronization.

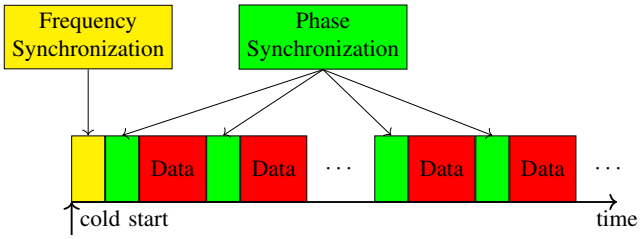

Fig. 4: Synchronization procedure.

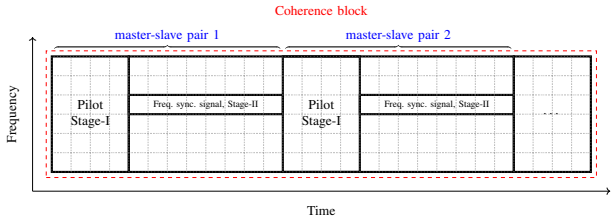

(a) Frequency Synchronization.

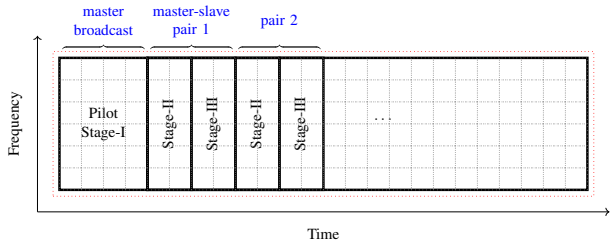

(b) Phase Synchronization.

Fig. 5: An example of resource allocation in OFDM resource grid for synchronization.

C. Frequency Synchronization Among Multiple APs

In this section, we extend the BeamSync frequency synchronization algorithm to the case of multiple APs. We consider the same scenario as in Sec. III-D. The BeamSync protocol for frequency synchronization among multiple APs is illustrated in Fig. 3. The slave APs synchronize with the master AP in a sequential fashion. In each synchronization slot, the slave AP sends the pilot to the master AP for the estimation of the dominant direction of the received signal (stage-I). Then the master sends the frequency synchronization signal to the slave AP for the estimation of the frequency offset.

D. BeamSync Protocol

In a distributed system, the APs are likely to be out of synchronization during the cold start and require a synchronization stage before users can communicate with the APs. This synchronization stage requires dedicated resources for synchronization of the APs, which need to be allocated prior to transmission to/from the users. Therefore, the current architecture needs to be redesigned to accommodate this requirement. After the initial power-up, all the APs will synchronize the frequency and the phase with a master AP in a sequential fashion using the BeamSync protocol. After the synchronization stage, regular data transmission stage with users take place, which include channel estimation, uplink and downlink data transmission. The synchronization procedure needs to be done when the APs go out of synchronization. Due to the presence of phase noise in the transceivers, phase synchronization needs to be done more often compared to frequency synchronization. The synchronization procedure dispersed over time is represented in Fig. 4.

Fig. 5 shows an example of resource allocation for synchronization in an OFDM resource grid. For frequency synchronization, the synchronization signal is sent over different time intervals to capture the phase shifts occurring over time due to the frequency offset. Resources for pilot signaling and frequency synchronization signal are allocated for each master-slave pair in a coherence block for frequency synchronization. In the case of phase synchronization, the resources allocated for pilot can be used by all the slave APs who are synchronizing in the same coherence interval. Afterward, resources for stage-II and stage-III are dedicated for each master-slave pair.

As the number of APs increases in a distributed system, the time required for synchronization also increases. Additionally, if the APs are spread over a wide geographic area, some of them may not be able to communicate with each other which limits the current algorithm for large area synchronization. In this situation, one possible approach could be to consider a clustering approach, where the APs in each cluster form an independent distributed system, but we leave this for potential future work.

V. Simulations

In this section, we discuss the performance of the proposed BeamSync protocol for synchronization in distributed massive MIMO systems. The BeamSync algorithm does not rely on any particular channel model: the algorithm is agnostic to the channel model and therefore to the array topology. All processing is done within single coherence intervals over which the channel is static. For simplicity we consider an independent Rayleigh block fading channel, i.e., each element of the channel matrix $\mathbf{G}$ is distributed as $\mathcal{CN}(0,1)$, thus, not modeling any particular antenna array configuration or topology. We consider a carrier frequency of 3 GHz, a signal bandwidth of 20 MHz and a symbol timing of $T = \frac{1}{14}$ ms for the simulations. Furthermore, we draw the transmit and receive channel gains at random from a $\mathcal{CN}(0,1)$ distribution. This makes the phase offsets uniformly random over $[0, 2\pi)$. We use 10^5 Monte Carlo trials for the simulations. The downlink rates from the APs to the users depend on the magnitude of the alignment error, but not on which specific synchronization method that was used for the alignment. Hence, when comparing different schemes, we chose the alignment error or the RMSE of the estimates as the performance metric.

In the system setup, we assume that all the antennas are driven by their own RF chain thereby enabling fully digital beamforming. Hence, BeamSync is a fully digital beamforming-based synchronization technique, which allows us to beamform the signal in any direction in a 3-dimensional environment. In this work, we consider fixed grid of beams (FGB) synchronization as the main benchmark scheme. In FGB, the transmitter performs transmit beamforming and the receiver performs receive beamforming from a fixed set of available beamforming directions. FGB is implemented with a single RF chain driving all antennas, and thus, is an analog beamforming technique. In our simulations, we consider the columns of a discrete Fourier transform (DFT) matrix as the set of orthogonal beams. Let $\{\mathbf{f}_{A,k} \in \mathbb{C}^{M_A \times 1},\ k = 1, 2, \cdots, M_A\}$ be the fixed set of beams available at the AP A. The transmit and receive beamforming vectors are chosen such that the received signal power is maximized. Let

$$k = \underset{k'}{\operatorname{argmax}} \ \|\mathbf{f}_{A,k'}^{\mathrm{H}} \mathbf{Y}_A\|^2,\ l = \underset{l'}{\operatorname{argmax}} \ \|\mathbf{f}_{A,l'}^{\mathrm{H}} \mathbf{Y}_A\|^2. \quad (39)$$

Then, the transmit beamforming vector is chosen to be $\mathbf{a}_t = \mathbf{f}_{A,k}^*$, and the receive beamforming vector is $\mathbf{a}_r = \mathbf{f}_{A,l}$ for AP A. Synchronization with the FGB scheme does not require estimation of the channel between the APs, and does not require sending measurement data to the CPU. Thus, we use the FGB scheme for comparison with BeamSync. Note that FGB results in the reception of a scalar quantity for each beam in the grid, rather than a vector quantity (measurements from all antennas) as for BeamSync. Unless there is phase coherency between different beams in the analog beamforming (which we do not assume), the analog beamforming would not allow for fully phase-coherent digital processing of the received pilots. Thus, with FGB, $M_A \times M_B$ measurements are needed to determine the best transmit and receive beamforming vectors. In contrast, with BeamSync, the beamforming vector is obtained from L measurements (length of the pilot signal) and computation of the dominant eigenvector of the measurement matrix.

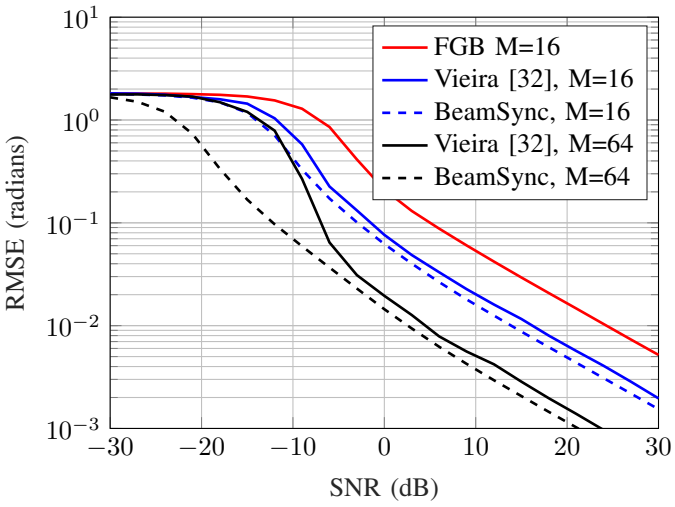

Fig. 6: Comparison of BeamSync with other reciprocity calibration methods. For this plot, the parameters considered are $M = M_A = M_B$, $L = M$, and $N = \frac{M}{2}$.

A. Phase Synchronization

For simulations, we have experimented with different phase synchronization signals, viz. (i) a complex Gaussian signal, (ii) an all-one signal, and (iii) a sinusoidal signal, all with the same norm $\|\mathbf{x}\|^2 = N$. The Monte-Carlo performance of BeamSync with the above signals were indistinguishable. Thus, the changes in noise covariance had more or less no effect on the performance. For the plots, we have used the complex Gaussian signal as the phase synchronization signal. In Fig. 6, we show the superiority of the BeamSync over the calibration method for distributed massive MIMO proposed in [32] (which to our knowledge is state-of-the-art) and over the FGB scheme. For the plot, we consider $M = M_A = M_B$. We consider a modified version of [32] such that all the antennas at AP-A and AP-B are equipped with RF chains. Thus, the algorithm in [32] requires $2M$ measurements with the modified scheme (M measurements in each direction). Note that, the original paper [32] considers analog beamforming with one RF chain per AP and hence, requires $2M^2$ measurements. For a fair comparison, in BeamSync we consider $L = M$ and $N = \frac{M}{2}$, thereby requiring a total of $2M$ measurements. We keep the total energy and resources spent for transmission the same in all schemes. From the figure, it can be seen that BeamSync performs 3 dB better. Also, BeamSync performs much better at low SNR compared to the FGB and [32] schemes. Note that the approach in [32] is centralized, and requires the measurement data from APs to be sent to the CPU through fronthaul. In contrast, BeamSync does not require any measurement data to be sent to the CPU and the APs can estimate their phase offsets independently.

Fig. 7 shows the performance of BeamSync protocol for phase synchronization in distributed massive MIMO systems. It can be seen from the figure that, the simple estimator in (10)

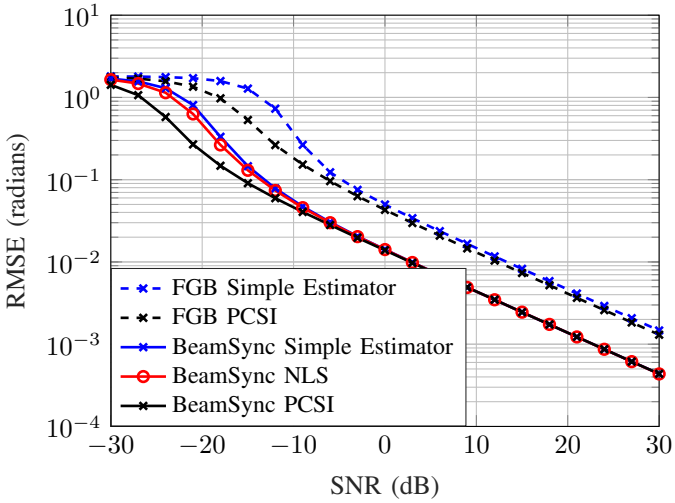

Fig. 7: BeamSync performance for phase estimates with $M_A = M_B = 16$, $L = 16$, and $N = 100$.

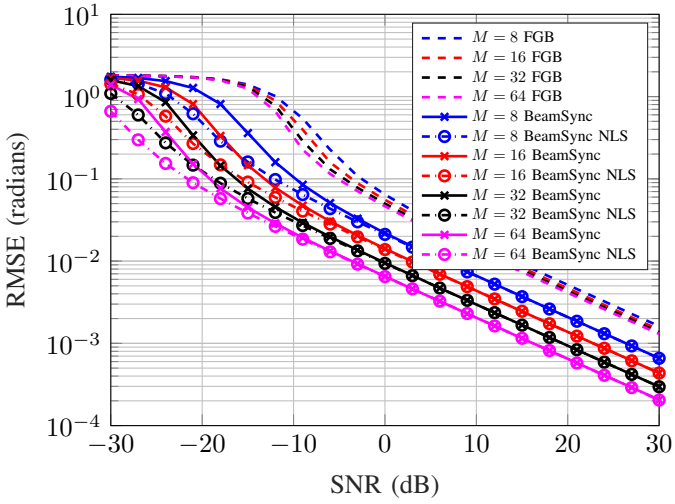

Fig. 8: BeamSync performance for phase estimates for different number of antennas, $M_A = M_B = M$, $L = M$, and $N = 100$.

performs equally well as the optimal estimator at high SNR. Moreover, at high SNR, the performance of the estimators approaches the performance of the estimator if we had perfect channel state information (PCSI). Thus, by using BeamSync with the simple estimator in (10), the synchronization can be done without estimating the channel between the APs. For a fixed RMSE requirement, the BeamSync protocol has an SNR gain of 10 dB when compared with the FGB scheme.

Fig. 8 shows the phase estimation performance of BeamSync for different numbers of antennas with NLS and with the simple estimator. It can be seen from the plot that the BeamSync performance improves with the number of antennas at the AP. The performance of the simple estimator matches with the NLS and hence, BeamSync can perform well without knowledge of the channel between the APs. For every doubling of the number of antennas, the performance of BeamSync

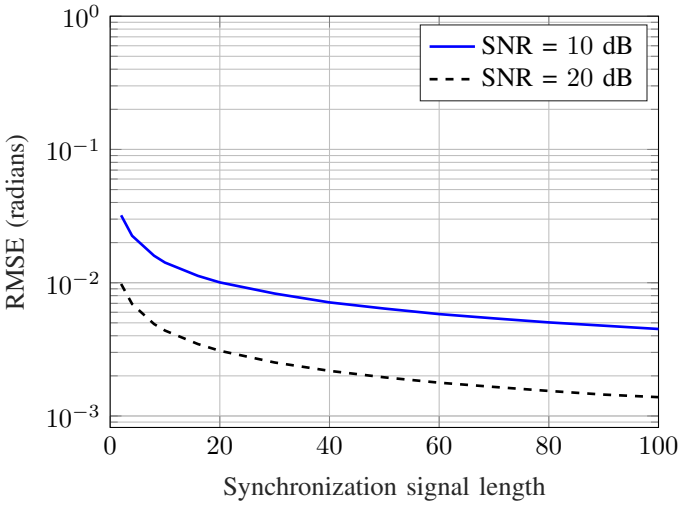

Fig. 9: BeamSync performance with the synchronization signal length for different SNR levels. $M_A = M_B = 16$ and $L = 16$.

improves by 3 dB. This is due to the increase in the SNR by beamforming and spatial processing gain. The improvement in the FGB scheme is negligible.

The estimation performance of BeamSync for different synchronization signal sequence lengths is provided in Fig. 9. The performance improves with the synchronization signal length.

B. Phase Noise

A practical LO driving the RF chain will experience phase fluctuations creating non-negligible distortions in the transmit signal. This is referred to as *phase noise* and is widely studied in [36]–[39]. We consider all the RF chains in an AP to be driven by a single LO and thus, operate in synchronous mode. Let ω_A be the phase noise process at AP A. We use the widely accepted discrete Wiener phase noise model [38], [39] given by

$$\omega_A[n+1] = \omega_A[n] + \nu_A[n], \tag{40}$$

where the increments $\nu_A[n]$ are i.i.d. zero mean Gaussian random variables, i.e., $\nu_A[n] \sim \mathcal{N}(0, \sigma_\nu^2)$. The variance $\sigma_\nu^2 = 4\pi^2 f_c^2 c_{vco} T_s$, where f_c is the carrier frequency, T_s is the sampling interval and c_{vco} is a constant which determines the quality of a LO. Let ω_B be the phase noise process at AP B. Without loss of generality we can assume $\omega_A[1] = \omega_B[1] = 0$, as it could be captured into t_1^A and t_1^B, respectively. Let $\omega[n] = \omega_A[n] + \omega_B[n]$ such that the increments of ω are distributed as $\mathcal{N}(0, 2\sigma_\nu^2)$. Let

$$\boldsymbol{\omega}_p^q = \left[e^{j\omega[p]} \; e^{j\omega[p+1]} \; \cdots \; e^{j\omega[q]}\right]^{\mathrm{T}}. \tag{41}$$

The phase noise effects at the receiving APs can be modeled into our signal model as follows:

$$\mathbf{Y}_{B1} = \sqrt{L}\frac{t_1^A}{r_1^A}\mathbf{G}_e^{\mathrm{T}}\mathbf{\Phi}^{\mathrm{H}}\mathbf{D}_{\boldsymbol{\omega}_1^L} + \mathbf{W}_{B1} \tag{42}$$

$$\mathbf{Y}_{A1} = \frac{t_1^B}{r_1^B}\mathbf{G}_e\mathbf{a}\mathbf{x}^{\mathrm{T}}\mathbf{D}^{\mathrm{H}}_{\boldsymbol{\omega}_{L+1}^{L+N}} + \mathbf{W}_{A1} \tag{43}$$

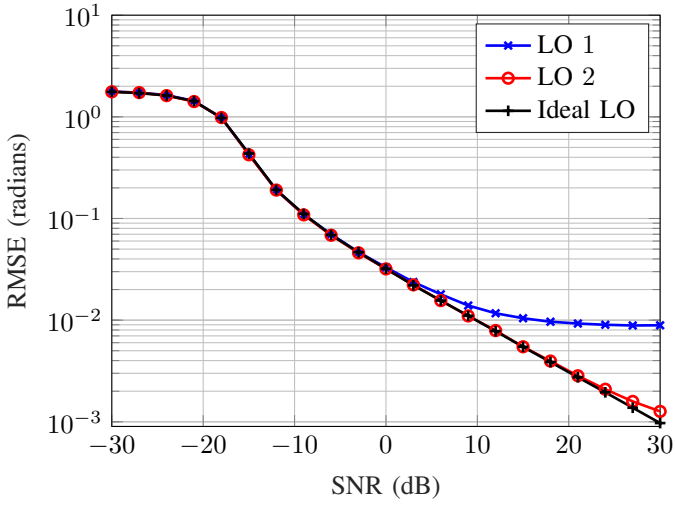

Fig. 10: BeamSync performance for phase estimates for different LOs with $M_A = M_B = 16$, $L = 16$, and $N = 20$.

$$\mathbf{Y}_{B2} = \sqrt{c}\frac{t_1^A}{r_1^A}\mathbf{G}_e^{\mathrm{T}}\mathbf{Y}_{A1}^{*}\mathbf{D}_{\boldsymbol{\omega}_{L+N+1}^{L+2N}} + \mathbf{W}_{B2}. \tag{44}$$

Fig. 10 shows the phase estimation performance of the BeamSync in the presence of phase noise at the estimating APs. We consider two crystal oscillators: LO 1 with $c_{vco} = 1.7610 \times 10^{-19}$ (rad Hz)$^{-1}$, and LO 2 with $c_{vco} = 1.4647 \times 10^{-21}$ (rad Hz)$^{-1}$, where the latter is a high-performance LO. We compare the performance of the above two LOs with an ideal LO with no phase-noise. From the plot, BeamSync can perform well in the presence of phase noise. By using a high performing LO, the performance can be improved further. Note that a free-running voltage controlled oscillator (VCO) can experience unbounded phase noise, which can cause significant synchronization issues in a distributed system. However, in practical systems, phase locked loops (PLLs) are typically used in conjunction with the VCO to stabilize the phase noise. As a result, the phase offset between the APs will drift slowly over time, and the amount of drift will depend on the operating environment of the APs.

C. Impact of Reciprocity Calibration Errors

Cellular massive MIMO with a single AP relies on the assumption of channel reciprocity and reciprocity calibration suffices to achieve this [3], [11]. A per-AP reciprocity calibration method was provided in [11], wherein it was also demonstrated experimentally that the reciprocity calibration can be performed rather infrequently (on the time-scale of hours). In contrast, in distributed MIMO systems, if the APs are driven by independent LOs, then in addition to the per-AP reciprocity calibration errors, the system will also experience phase drifts between the APs (on a much faster time-scale). Our BeamSync algorithm is a procedure to synchronize the phase between independently operating APs, but not a method to achieve per-AP reciprocity calibration. In fact, BeamSync relies on the APs being individually reciprocity-calibrated.

There are two consequences of per-AP reciprocity errors: first, that some beamforming gain is lost when serving UEs; second, as a quantitatively much smaller effect, that the beamforming between the APs inside of the BeamSync algorithm loses some efficiency which in turn impacts, although very little, the phase synchronization performance – which in turn affects the beamforming gain when serving UEs.

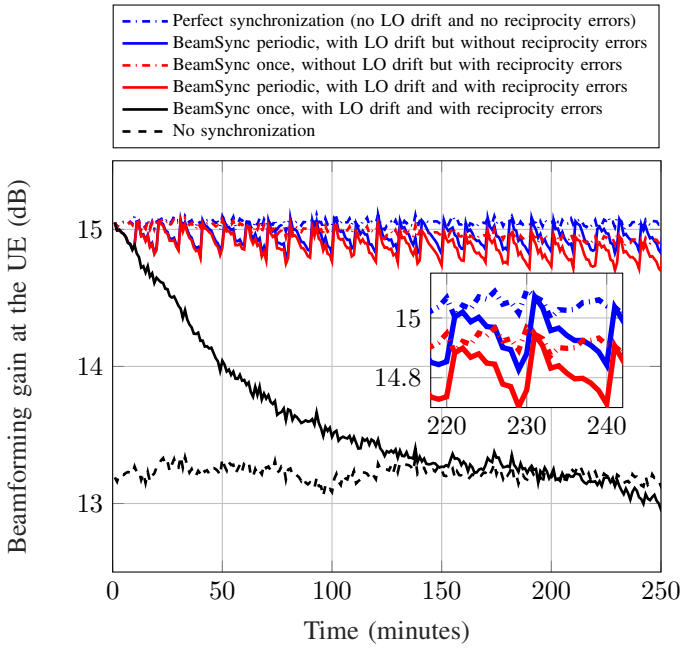

Fig. 11: Time evolution of beamforming gain at the UE from APs A & B. Here $M_A = M_B = 16$, $L = 16$, $N = 20$, and SNR= 20 dB.

To give a numerical illustration of the above phenomena, we model the per-AP reciprocity calibration errors as additive Gaussian with zero mean and variance of σ_ϵ^2. We take, from the experimental results in [11], $\sigma_\epsilon^2 = 10^{-9.6}$, yielding a mean angle deviation of 2.7% over 4 hours of time. We ignore the variations in amplitude as the measurements in [11] show only tiny variations (0.7%) in the amplitude over the same time duration. This means that the per-AP reciprocity calibration coefficients $\{\frac{t_m^A}{r_m^A}\}$ for AP A and $\{\frac{t_m^B}{r_m^B}\}$ for AP B vary very slowly over time. However, the ratio $\frac{t_1^A}{r_1^A}/\frac{t_1^B}{r_1^B}$ changes must faster, due to the LO drifts [40]. For the simulations, we consider that both the APs are equipped with a high-quality LO, specifically LO 2 (see its performance figures in Section V-B). Practical deployments may use LOs of less quality, which entails much more frequent re-calibration; we use LO 2 here only to improve readability of the plots.

To study the consequences of per-AP reciprocity errors and LO drift, we consider how the beamforming gain achieved at the UE evolves over time. We refer to Fig. 1 for the definition of all quantities being referred to in the following. For simplicity, we consider that both APs are at the same distance from the UE, and that the channels $\mathbf{g}_A$ and $\mathbf{g}_B$ are Rayleigh fading with i.i.d. $\mathcal{CN}(0,1)$ entries. Fig. 11 shows the beamforming gain at the UE over time. In the simulation, BeamSync calibration is done once (at time 0) for some of the curves, and periodically thereafter for some of curves. We

observe the following:

1) For reference (blue dash-dotted curve), we consider the scenario where we have perfect phase synchronization between the APs (this is equivalent to no LO drift or noise) as well as no per-AP reciprocity calibration errors. This achieves the maximum possible beamforming gain, $M_A + M_B$.
2) In the presence of LO drift but with BeamSync performed only once (no periodic re-synchronization between the APs), the beamforming gain drops rapidly over time (black solid curve). For a lower-quality LOs, e.g., LO 1, this drop in the gain would be much faster. This illustrates that periodic phase re-synchronization is required.
3) With LO drift and BeamSync phase calibration performed periodically every 10 minutes, but *without* per-AP reciprocity calibration errors (blue solid curve): In this case, BeamSync periodic re-calibration helps to maintain a good beamforming gain. The re-calibration recovers the losses from the phase drift between the APs. The zig-zag behaviour in the plot is due to the loss of synchronization during the 10-minute interval. In practice, the periodicity of BeamSync re-calibration depends on the quality of the LO used.
4) With LO drift and BeamSync phase calibration performed periodically every 10 minutes, and *with* per-AP reciprocity calibration errors (red solid curve): BeamSync is able to recover the losses from the LO drift; however, it is unable to recover the long-term losses from per-AP reciprocity calibration errors.
5) Also for reference, we consider a hypothetical situation where we have no LO drift, but we do have per-AP reciprocity calibration errors (red dash-dotted curve). Refer to the inset for better clarity.

When executing the BeamSync procedure to phase-synchronize two APs, the per-AP reciprocity error will impact the synchronization performance (as already noted above). To illustrate this effect, Fig. 12 shows the time evolution of the mean absolute value of the phase difference between the APs seen at the UE after phase correction is applied at AP B. Per-AP reciprocity calibration is done once, at time 0. The gap between the red solid curve with square markers and black solid curve with diamond markers shows the angle deviation between the APs caused by the per-AP reciprocity calibration errors inside the BeamSync algorithm. It can be seen from the plot that BeamSync causes a tiny deviation of $\phi \approx 1.5^\circ$ after 4 hours due to the reciprocity errors inside the BeamSync algorithm. This leads to a beamforming loss by a factor of $\frac{M_A+M_B}{|M_A+e^{j\phi}M_B|}$, which for the example considered in Fig. 12 is 0.0004 dB. This loss should be compared to the beamforming loss in Fig. 11 (the 0.13 dB gap between blue and red dash-dotted curves at 4 hours). The 0.13 dB gap in Fig. 11 is due to the loss of beamforming gain due to reciprocity errors *and* the loss of BeamSync performance due to reciprocity errors; the latter amounts to only 0.0004 dB of the 0.13 dB in total (this is the second consequence of the reciprocity calibration errors).

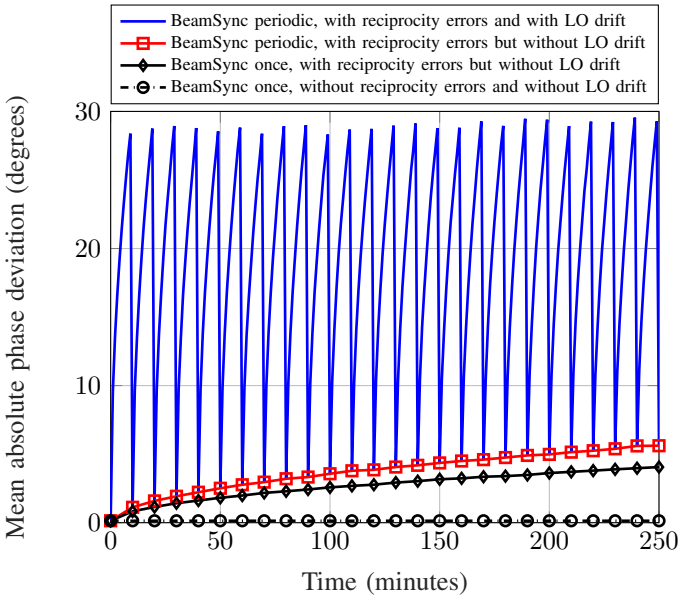

Fig. 12: Time evolution of the mean of the absolute phase deviation between the APs observed at the UE. Here $M_A = M_B = 16$, $L = 16$, $N = 20$, SNR$= 20$ dB.

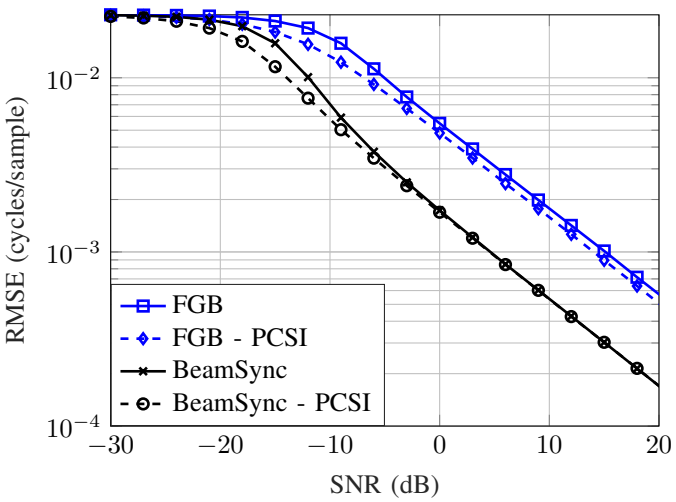

Fig. 13: BeamSync performance for carrier frequency offset estimates with $M_A = M_B = 16$, $L = 16$, and $N_f = 10$.

D. Frequency Synchronization

In this subsection, we consider the frequency synchronization performance of the BeamSync. As per the 3GPP TS 38.104, the carrier frequency of the AP shall be accurate within ± 0.05 ppm. Thus, for 3 GHz carrier frequency, we assume that the simulated frequency offset Δ ranges uniformly from -300 Hz to 300 Hz. Here we consider the RMSE $= \sqrt{\mathbb{E}\left\{\left\|\Delta T - \hat{\Delta} T\right\|^2\right\}}$ (cycles/sample) as the performance metric. We have considered a sinusoidal signal as the frequency synchronization signal. The frequency synchronization performances of BeamSync and the fixed grid of beams are shown in Fig. 13 and Fig. 14. The gains achieved for frequency synchronization are similar to the gains in phase

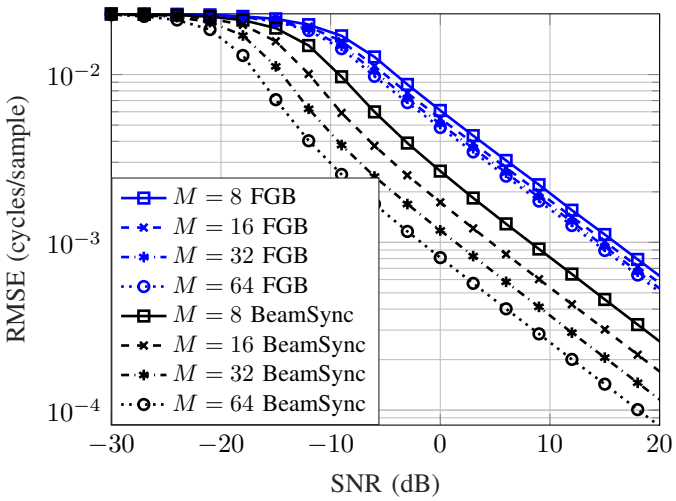

Fig. 14: BeamSync performance for carrier frequency offset estimates with $M_A = M_B = M$, $L_B = M_B$ and $N_f = 10$.

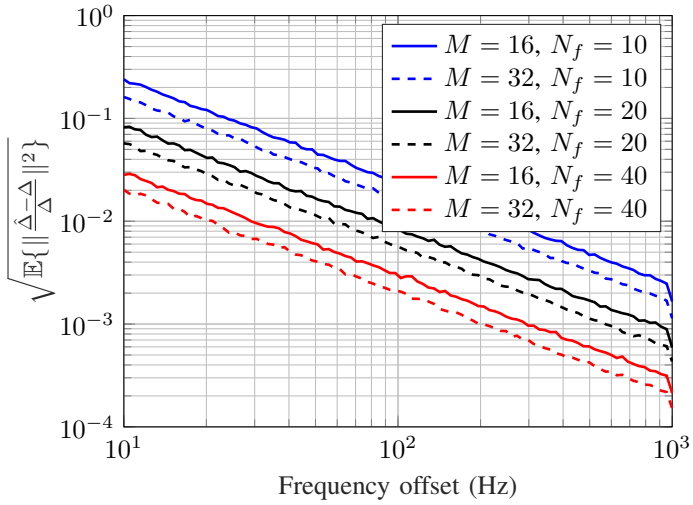

Fig. 15: BeamSync performance with frequency offset range. $M_A = M_B = M$ and $L = M$ and SNR $= 20$ dB.

synchronization. For example, for a fixed RMSE requirement, the SNR gain is approximately 10 dB for BeamSync compared to the FGB scheme. Also, it can be seen that for a fixed RMSE requirement, the SNR requirement reduces by 3 dB when the number of antennas is doubled at the APs for the BeamSync protocol.

Fig. 15 shows the performance of BeamSync with respect to the frequency offset. For a coarse synchronization, we need less synchronization signal length N_f, while for fine synchronization we need larger N_f, or a larger number of antennas, or a higher SNR. By doubling N_f, the SNR improves by 6 dB.

Fig. 16 shows the phase estimation performance of BeamSync when we have a residual frequency offset Δ between two APs. A residual frequency error between APs can lead to a significant change in phase with time, which impacts the phase estimation. Hence, it is necessary to correct the phases soon after frequency synchronization. With perfect frequency synchronization, i.e., $\Delta = 0$, the phase estimation RMSE

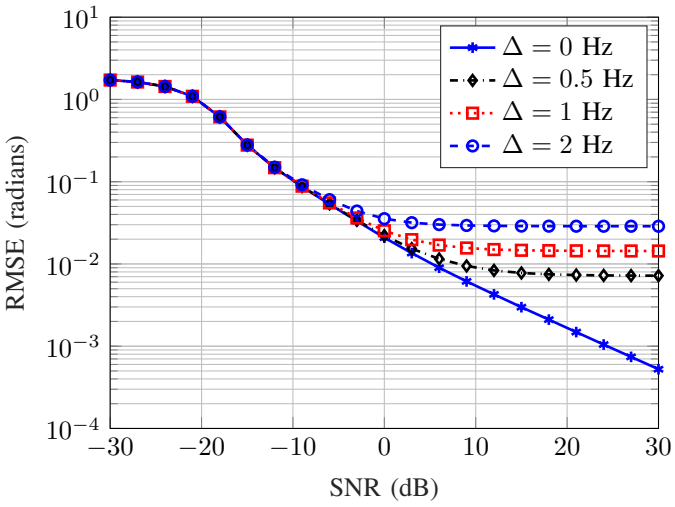

Fig. 16: BeamSync phase synchronization performance with imperfect frequency offset. $M_A = M_B = 32$, $L = 32$ and $N = 32$.

decreases as the SNR increases. However, with residual frequency errors, the RMSE reaches a constant floor independent of the SNR. Furthermore, this constant value increases as the residual frequency error increases. To synchronize faster, different AP pairs can use frequency division multiple access (FDMA) to mitigate the issue of imperfect frequency offsets. If the number of AP pairs to be synchronized is large, we need to interlace frequency and phase synchronization between different pairs.

VI. Conclusion

In this paper, we studied the synchronization requirements in a distributed massive MIMO from a reciprocity perspective. We proposed two novel over-the-air synchronization protocols, BeamSync, based on digital beamforming to synchronize the carrier frequency offsets and phase offsets among distributed APs. We analytically derived the optimal frequency offset estimator and phase offset estimators. We perform a phase calibration of reciprocity-calibrated APs with one AP to enable coherent transmission and also propose a simpler phase offset estimator which performs close to the optimal estimator at high SNR. We analytically showed that the synchronization signals need to be beamformed in the dominant direction of the effective channel in which the signal is received. BeamSync can achieve a 3 dB gain for every doubling of the number of antennas at the APs. This performance is due to the improved SNR by beamforming and spatial processing gain.

Appendix

In this appendix, we briefly layout how reciprocity calibration is obtained at a multi-antenna AP [11]. Consider two antennas jointly serving a UE as shown in Fig. 17. Let g_1 be the reciprocal channel between the UE and antenna 1, and similarly g_2 be the reciprocal channel between the UE and antenna 2. Let t_1, t_2 be the RF transmit chain gains at antennas 1 and 2, respectively. Also, in a similar way, we define r_1, r_2

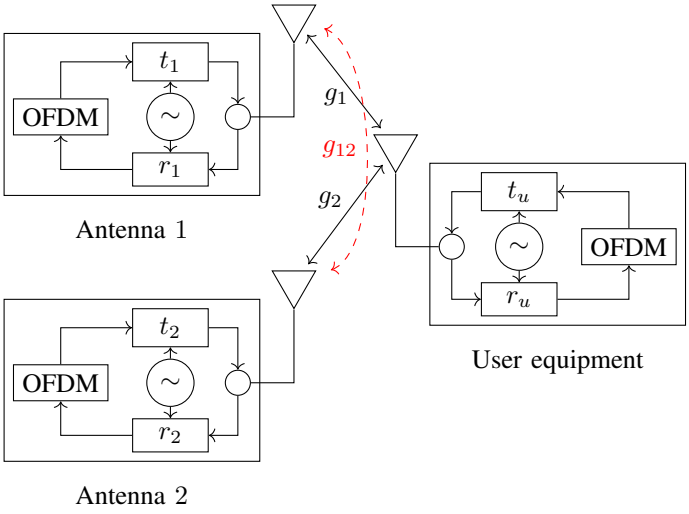

Fig. 17: System model with 2 antennas serving a UE.

as the RF receive chain gains at antennas 1 and 2, respectively. The two uplink channels are given by

$$g_{u1}^{\text{UL}} = t_u \; g_1 \; r_1 \tag{45}$$
$$g_{u2}^{\text{UL}} = t_u \; g_2 \; r_2. \tag{46}$$

Similarly, the downlink channels are given by

$$g_{1u}^{\text{DL}} = t_1 \; g_1 \; r_u \tag{47}$$
$$g_{2u}^{\text{DL}} = t_2 \; g_2 \; r_u. \tag{48}$$

With pilot signaling from the UE, antennas 1 and 2 can estimate the uplink channels g_{u1}^{UL} and g_{u2}^{UL}, respectively. On the downlink, both the antennas 1 and 2 applies *conjugate beamforming* [3] and the total channel gains seen by the UE from both antennas are given by

$$h_1 = \left(g_{u1}^{\text{UL}}\right)^* g_{1u}^{\text{DL}} = t_u^* r_1^* \left|g_1\right|^2 t_1 r_u \tag{49}$$
$$h_2 = \left(g_{u2}^{\text{UL}}\right)^* g_{2u}^{\text{DL}} = t_u^* r_2^* \left|g_2\right|^2 t_2 r_u. \tag{50}$$

The channel gains h_1 and h_2 can be written in terms of amplitude and phase differences of RF chains as follows

$$\begin{aligned} h_1 &= \left|t_u\right| \left|r_1\right| \left|g_1\right|^2 \left|t_1\right| \left|r_u\right| e^{j((\angle t_1 - \angle r_1) - (\angle t_u - \angle r_u))} \\ h_2 &= \left|t_u\right| \left|r_2\right| \left|g_2\right|^2 \left|t_2\right| \left|r_u\right| e^{j((\angle t_2 - \angle r_2) - (\angle t_u - \angle r_u))}. \end{aligned} \tag{51}$$

Note that in (51) the phase shifts caused by the reciprocal channels g_1 and g_2 are removed through conjugate beamforming. For the signals from antennas 1 and 2 to add up coherently at UE, the phases of h_1 and h_2 need to be precompensated at the antennas. A relative compensation of antenna 2 with antenna 1 suffices to add up the signals at the UE coherently. Mathematically, what matters is the difference between the phases of two antennas, i.e., $((\angle t_1 - \angle r_1) - (\angle t_2 - \angle r_2))$. If we have many antennas, then we need to relatively precompensate the phases of all antennas with antenna 1, i.e., compensate $((\angle t_1 - \angle r_1) - (\angle t_i - \angle r_i))$ for $i = 2, 3, \cdots$.

Now, consider two antennas 1 and 2, and let $g_{12} \in \mathbb{C}$ be the reciprocal channel gain between them. Using a bidirectional measurement between antennas 1 and 2, we obtain

$$z_{12} = t_1 g_{12} r_2 = \left|t_1\right| \left|g_{12}\right| \left|r_2\right| e^{j(\angle t_1 + \angle g_{12} + \angle r_2)} \tag{52}$$
$$z_{21} = t_2 g_{12} r_1 = \left|t_2\right| \left|g_{12}\right| \left|r_1\right| e^{j(\angle t_2 + \angle g_{12} + \angle r_1)}. \tag{53}$$

Dividing these two measurements we get

$$\frac{z_{12}}{z_{21}} = \frac{\left|t_1\right| \left|r_2\right|}{\left|t_2\right| \left|r_1\right|} e^{j((\angle t_1 - \angle r_1) - (\angle t_2 - \angle r_2))}. \tag{54}$$

Thus, with (54), antenna 2 can precompensate the phase, so as to have coherent combining of the signals at the UE and we obtain the overall channel gain from antenna 2 as

$$\begin{aligned} \frac{z_{12}}{z_{21}} h_2 &= \frac{\left|t_1\right| \left|r_2\right|}{\left|t_2\right| \left|r_1\right|} e^{j((\angle t_1 - \angle r_1) - (\angle t_2 - \angle r_2))} \\ &\quad \times \left|t_u\right| \left|r_2\right| \left|g_2\right|^2 \left|t_2\right| \left|r_u\right| e^{j((\angle t_2 - \angle r_2) - (\angle t_u - \angle r_u))} \\ &= \frac{\left|t_1\right| \left|r_u\right|}{\left|r_1\right| \left|t_u\right|} \left|t_u\right|^2 \left|g_2\right|^2 \left|r_2\right|^2 e^{j((\angle t_1 - \angle r_1) - (\angle t_u - \angle r_u))}. \end{aligned} \tag{55}$$

Thus, for many antennas, we could perform bidirectional measurements of all antennas $(2, 3, \cdots)$ with antenna 1 and obtain the calibration coefficients of all the antennas. For a collocated AP, where all the antennas are at the same unit, the channels between the antennas remain same for a long duration of time. Moreover, as all the antennas in the AP share the clocks, the internal calibration coefficients obtained are stable for longer periods of time. Hence, calibrating the antennas in a collocated setup can be done very infrequently [11].

REFERENCES

[1] U. K. Ganesan, R. Sarvendranath, and E. G. Larsson, "Beamsync: Over-the-air carrier synchronization in distributed radioweaves," in *25th International ITG Workshop on Smart Antennas (WSA)*, 2021, pp. 1–6.

[2] T. L. Marzetta, "Noncooperative cellular wireless with unlimited numbers of base station antennas," *IEEE Transactions on Wireless Communications*, vol. 9, no. 11, pp. 3590–3600, Nov. 2010.

[3] T. L. Marzetta, E. G. Larsson, H. Yang, and H. Q. Ngo, *Fundamentals of massive MIMO*. Cambridge University Press, 2016.

[4] V. Chandrasekhar, J. G. Andrews, and A. Gatherer, "Femtocell networks: A survey," *IEEE Communications Magazine*, vol. 46, no. 9, pp. 59–67, 2008.

[5] H. Q. Ngo, A. Ashikhmin, H. Yang, E. G. Larsson, and T. L. Marzetta, "Cell-free massive MIMO versus small cells," *IEEE Transactions on Wireless Communications*, vol. 16, no. 3, pp. 1834–1850, Mar. 2017.

[6] G. Foschini, "The value of coherent base station coordination," in *Conference on Information Sciences and Systems (CISS), Johns Hopkins University*, Mar 2005.

[7] M. K. Karakayali, G. J. Foschini, and R. A. Valenzuela, "Network coordination for spectrally efficient communications in cellular systems," *IEEE Wireless Communications*, vol. 13, no. 4, pp. 56–61, 2006.

[8] G. Caire, S. A. Ramprashad, and H. C. Papadopoulos, "Rethinking network MIMO: Cost of CSIT, performance analysis, and architecture comparisons," in *Information Theory and Applications Workshop (ITA)*, 2010, pp. 1–10.

[9] D. Gesbert, S. Hanly, H. Huang, S. S. Shitz, O. Simeone, and W. Yu, "Multi-cell MIMO cooperative networks: A new look at interference," *IEEE journal on selected areas in communications*, vol. 28, no. 9, pp. 1380–1408, 2010.

[10] G. Interdonato, E. Björnson, H. Quoc Ngo, P. Frenger, and E. G. Larsson, "Ubiquitous cell-free massive MIMO communications," *EURASIP Journal on Wireless Communications and Networking*, vol. 2019, no. 197, pp. 1–13, 2019.

[11] C. Shepard, H. Yu, N. Anand, E. Li, T. Marzetta, R. Yang, and L. Zhong, "Argos: Practical many-antenna base stations," in *Proceedings of the 18th annual international conference on Mobile computing and networking*, 2012, pp. 53–64.

[12] B. M. Lee, "Calibration for channel reciprocity in industrial massive MIMO antenna systems," *IEEE Transactions on Industrial Informatics*, vol. 14, no. 1, pp. 221–230, 2017.
[13] C.-M. Chen, S. Blandino, A. Gaber, C. Desset, A. Bourdoux, L. Van der Perre, and S. Pollin, "Distributed massive MIMO: A diversity combining method for TDD reciprocity calibration," in *2017 IEEE Global Communications Conference*. IEEE, 2017, pp. 1–7.
[14] N.-I. Kim, C. W. Yu, S.-E. Hong, J.-H. Na, and B. C. Chung, "A gradual method for channel non-reciprocity calibration in cell-free massive MIMO," *IEEE Communications Letters*, vol. 26, no. 11, pp. 2779–2783, 2022.
[15] *GSM Recommendation 05.01: Physical Layer on Radio Path*. ETSI, 1998.
[16] P. H. Moose, "A technique for orthogonal frequency division multiplexing frequency offset correction," *IEEE Transactions on Communications*, vol. 42, no. 10, pp. 2908–2914, Oct. 1994.
[17] T. M. Schmidl and D. C. Cox, "Robust frequency and timing synchronization for OFDM," *IEEE Transactions on Communications*, vol. 45, no. 12, pp. 1613–1621, Dec. 1997.
[18] D. Huang and K. B. Letaief, "Carrier frequency offset estimation for OFDM systems using null subcarriers," *IEEE Transactions on Communications*, vol. 54, no. 5, pp. 813–823, May 2006.
[19] H. Huh, A. M. Tulino, and G. Caire, "Network MIMO with linear zero-forcing beamforming: Large system analysis, impact of channel estimation, and reduced-complexity scheduling," *IEEE Transactions on Information Theory*, vol. 58, no. 5, pp. 2911–2934, 2011.
[20] S. A. Ramprashad and G. Caire, "Cellular vs. Network MIMO: A comparison including the channel state information overhead," in *IEEE 20th International Symposium on Personal, Indoor and Mobile Radio Communications*, 2009, pp. 878–884.
[21] F. Boccardi, H. Huang, and A. Alexiou, "Network MIMO with reduced backhaul requirements by MAC coordination," in *42nd Asilomar Conference on Signals, Systems and Computers*, 2008, pp. 1125–1129.
[22] P. Marsch and G. Fettweis, "On base station cooperation schemes for downlink network MIMO under a constrained backhaul," in *IEEE Global Telecommunications Conference*, 2008, pp. 1–6.
[23] Y.-S. Tu and G. J. Pottie, "Coherent cooperative transmission from multiple adjacent antennas to a distant stationary antenna through AWGN channels," in *IEEE 55th Vehicular Technology Conference*, vol. 1, 2002, pp. 130–134.
[24] R. Mudumbai, D. R. B. Iii, U. Madhow, and H. V. Poor, "Distributed transmit beamforming: challenges and recent progress," *IEEE Communications Magazine*, vol. 47, no. 2, pp. 102–110, 2009.
[25] M. M. Rahman, H. E. Baidoo-Williams, R. Mudumbai, and S. Dasgupta, "Fully wireless implementation of distributed beamforming on a software-defined radio platform," in *Proceedings of the 11th international conference on Information Processing in Sensor Networks*, 2012, pp. 305–316.
[26] F. Quitin, U. Madhow, M. M. U. Rahman, and R. Mudumbai, "Demonstrating distributed transmit beamforming with software-defined radios," in *IEEE International Symposium on a World of Wireless, Mobile and Multimedia Networks (WoWMoM)*, 2012, pp. 1–3.
[27] F. Quitin, M. M. U. Rahman, R. Mudumbai, and U. Madhow, "Distributed beamforming with software-defined radios: frequency synchronization and digital feedback," in *IEEE Global Communications Conference (GLOBECOM)*, 2012, pp. 4787–4792.
[28] H. V. Balan, R. Rogalin, A. Michaloliakos, K. Psounis, and G. Caire, "Airsync: Enabling distributed multiuser MIMO with full spatial multiplexing," *IEEE/ACM Transactions on Networking*, vol. 21, no. 6, pp. 1681–1695, Dec. 2013.
[29] M. Rahman, S. Dasgupta, and R. Mudumbai, "A distributed consensus approach to synchronization of RF signals," in *IEEE Statistical Signal Processing Workshop (SSP)*, 2012, pp. 281–284.
[30] O. Abari, H. Rahul, D. Katabi, and M. Pant, "Airshare: Distributed coherent transmission made seamless," in *IEEE Conference on Computer Communications (INFOCOM)*, 2015, pp. 1742–1750.
[31] R. Rogalin, O. Y. Bursalioglu, H. Papadopoulos, G. Caire, A. F. Molisch, A. Michaloliakos, V. Balan, and K. Psounis, "Scalable synchronization and reciprocity calibration for distributed multiuser MIMO," *IEEE Transactions on Wireless Communications*, vol. 13, no. 4, pp. 1815–1831, Apr. 2014.
[32] J. Vieira and E. G. Larsson, "Reciprocity calibration of distributed massive MIMO access points for coherent operation," in *IEEE 32nd Annual International Symposium on Personal, Indoor and Mobile Radio Communications (PIMRC)*, 2021, pp. 783–787.
[33] J. F. Epperson, *An introduction to numerical methods and analysis*. John Wiley & Sons, 2021.
[34] S. M. Kay, *Fundamentals of statistical signal processing*. Prentice Hall PTR, 1993.
[35] R. A. Horn and C. R. Johnson, *Matrix analysis*. Cambridge University Press, 2012.
[36] A. Demir, A. Mehrotra, and J. Roychowdhury, "Phase noise in oscillators: A unifying theory and numerical methods for characterization," *IEEE Transactions on Circuits and Systems I: Fundamental Theory and Applications*, vol. 47, no. 5, pp. 655–674, 2000.
[37] A. Mehrotra, "Noise analysis of phase-locked loops," *IEEE Transactions on Circuits And Systems—I: Fundamental Theory and Applications*, vol. 49, no. 9, p. 1309, 2002.
[38] S. Bittner, S. Krone, and G. Fettweis, "Tutorial on discrete time phase noise modeling for phase locked loops," 2008.
[39] A. Pitarokoilis, S. K. Mohammed, and E. G. Larsson, "Uplink performance of time-reversal MRC in massive MIMO systems subject to phase noise," *IEEE Transactions on Wireless Communications*, vol. 14, no. 2, pp. 711–723, Feb. 2014.
[40] R. Nissel, "Correctly modeling TX and RX chain in (distributed) massive MIMO-new fundamental insights on coherency," *IEEE Communications Letters*, 2022.

Unnikrishnan Kunnath Ganesan (S'20) received the Bachelor of Technology degree in Electronics and Communication Engineering from University of Calicut, Kerala, India in 2011 and the Masters in Engineering degree in Telecommunication Engineering from Indian Institute of Science, Bangalore, India in 2014. From 2014 to 2017, he worked as modem systems engineer with Qualcomm India Private Limited, Bangalore and from 2017 to 2019 he worked as senior firmware engineer with Intel. He is currently pursuing the Ph.D. degree with the Department of Electrical Engineering (ISY), Linköping University, Sweden. His primary research interests includes MIMO wireless communications, signal processing, and information theory.

Rimalapudi Sarvendranth (S'12-M'21) received his Bachelor of Technology degree in Electrical and Electronics Engineering from the National Institute of Technology Karnataka, Surathkal in 2009. He received his Master of Engineering and Ph.D. degrees from the Department of Electrical Communication Engineering, Indian Institute of Science, Bangalore in 2012 and 2020, respectively. He is currently working as an assistant professor in the Department of Electrical Engineering at the Indian Institute of Technology Tirupati. In 2021, he was a postdoctoral researcher in the Department of Electrical Engineering, at Linköping University, Sweden. He worked as an assistant professor in the Electronics and Electrical Engineering department of the Indian Institute of Technology Guwahati from January 2022 to June 2023. From 2012 to 2016, he was with Broadcom Communications Technologies, Bangalore, India, where he worked on the development and implementation of algorithms for LTE and IEEE 802.11ac wireless standards. His research interests include machine learning for wireless communication, multiple antenna techniques, spectrum sharing, and next-generation wireless standards.

Erik G. Larsson (S'99–M'03–SM'10–F'16) received the Ph.D. degree from Uppsala University, Uppsala, Sweden, in 2002. He is currently Professor of Communication Systems at Linköping University (LiU) in Linköping, Sweden. He was with the KTH Royal Institute of Technology in Stockholm, Sweden, the George Washington University, USA, the University of Florida, USA, and Ericsson Research, Sweden. His main professional interests are within the areas of wireless communications and signal processing. He co-authored *Space-Time Block Coding for Wireless Communications* (Cambridge University Press, 2003) and *Fundamentals of Massive MIMO* (Cambridge University Press, 2016).

He served as chair of the IEEE Signal Processing Society SPCOM technical committee (2015–2016), chair of the *IEEE Wireless Communications Letters* steering committee (2014–2015), member of the *IEEE Transactions on Wireless Communications* steering committee (2019-2022), General and Technical Chair of the Asilomar SSC conference (2015, 2012), technical co-chair of the IEEE Communication Theory Workshop (2019), and member of the IEEE Signal Processing Society Awards Board (2017–2019). He was Associate Editor for, among others, the *IEEE Transactions on Communications* (2010-2014), the *IEEE Transactions on Signal Processing* (2006-2010),and the *IEEE Signal Processing Magazine* (2018-2022).

He received the IEEE Signal Processing Magazine Best Column Award twice, in 2012 and 2014, the IEEE ComSoc Stephen O. Rice Prize in Communications Theory in 2015, the IEEE ComSoc Leonard G. Abraham Prize in 2017, the IEEE ComSoc Best Tutorial Paper Award in 2018, and the IEEE ComSoc Fred W. Ellersick Prize in 2019. He is a member of the Swedish Royal Academy of Sciences (KVA), and Highly Cited according to ISI Web of Science.